

Sub-diurnal variability of the carbon dioxide and water vapor isotopologues at the field observational scale

Jordi Vilà-Guerau de Arellano*, Gerbrand Koren, Huug G. Ouwersloot, Ivar van der Velde, Thomas Röckmann, John B. Miller

Institution, Wageningen 6700 AA, The Netherlands

ARTICLE INFO

Keywords:

CO₂
H₂O
Stable isotopologues
Sub-diurnal variability
Coupled soil-vegetation-atmosphere model
Harvard Forest observations
Boundary-layer dynamics

ABSTRACT

We investigated the sub-diurnal variability of the carbon dioxide and water vapour isotopologues by modelling a representative case measured above the Harvard Forest. To this end, we developed a model that couples the local processes governed by soil and vegetation conditions to non-local atmospheric processes such as entrainment and long-range advection. The model formulation is based on solving the stable isotopologues ¹²CO₂, ¹³CO₂, C¹⁸OO, H₂¹⁶O and H₂¹⁸O as conserved variables. It also includes simultaneously solving the meteorological state variables coupled with their respective surface fluxes. Our model results indicate the need for a comprehensive observational data-set to ensure that the essential processes and interactions between the boundary-layer dynamics of a forest and the atmospheric boundary layer are satisfactorily reproduced. We present and discuss the temporal evolution of the budgets of ¹³CO₂ and C¹⁸OO, in order to quantify the individual contributions made by soil, plant and entrainment dynamics. All these contributions turn out to be relevant, as they enable us to quantify how the energy, water and carbon fluxes on sub-daily scales are partitioned. Regarding the role played by entrainment, we carried out a set of three systematic experiments in which air, with different CO₂ and H₂O isotopic compositions originating in the residual layer, mix with the boundary-layer air. Our findings show that both the C¹⁸OO and H₂¹⁸O isotopic ratios and their respective isofluxes are influenced by the entrainment event. This result indicates that high frequency and accurate isotopologues surface measurements (seconds or minutes) can be used to quantify how non-local atmospheric processes modify isotopic composition at sub-daily scales.

1. Introduction

In understanding the coupling of processes that interact between the surface and the atmosphere (Monson and Baldocchi, 2014; Moene and van Dam, 2014), it is essential to be able to discriminate the individual contributions driven by soil, plants and the atmosphere. This is crucial to quantifying one of the largest uncertainties in weather and carbon-climate models: how the available radiative energy is used and partitioned to yield the heat, moisture and carbon surface fluxes (Trenberth et al., 2000). More specifically, the relationship between plant assimilation and transpiration determines water use efficiency (Lambers et al., 2008); and partitioning shifts between the sensible heat flux and evapotranspiration lead to modifications of the turbulent intensity and subsequent alterations in boundary-layer cloud formation (Vilà-Guerau de Arellano et al., 2012). Measurements and model representations of the carbon and water-stable isotopologues offer an unique perspective due to their different isotopic signature (Bowling et al., 2001) that enable to determine the contributions of soil, plants and entrainment to the flux partitioning. Our study adopts an integrative approach to

quantify the diurnal budgets of the stable isotopologues, with the aim of distinguishing between mechanisms controlled by surface (local) processes and those driven by non-local processes such as entrainment.

We therefore focus on studying the carbon and water vapour isotopologues at sub-daily (minutes) and sub-kilometre scales within the atmospheric boundary layer (ABL). It is at these spatiotemporal scales that the net fluxes of energy, water and carbon are measured, and they need to be accurately represented in weather and climate models (Bauer et al., 2015). By observing and modelling the stable isotopologues of carbon dioxide, CO₂ (defined as ¹²CO₂ + ¹³CO₂), ¹³CO₂ and C¹⁸OO, and atmospheric water vapour H₂O (defined as H₂¹⁶O + H₂¹⁸O) and H₂¹⁸O, we are able to quantify how the carbon dioxide and moisture fluxes respond to soil, plant and atmospheric conditions (Yakir and Sternberg, 2000; Griffis, 2013). As concluded by Wehr and Saleska (2015), the isotopic flux partitioning is useful in quantifying the contributions of the photosynthetic and respiratory components to the net ecosystem-atmosphere exchange. The various kinetic fractionation (diffusion-dependent) and equilibrium fractionation (thermodynamics-dependent) processes provide key information

* Corresponding author.

regarding the coupling between soil, leaf, plant and canopy processes that interact with the dynamics of the ABL. In particular, carbon dioxide discrimination is used as an indicator of differentiation of photosynthetic pathways due to sub-daily changes in the water vapour deficit and the photosynthetic active radiation (Bickford et al., 2009). Combining knowledge of carbon ^{13}C and oxygen ^{18}O enables us to connect the transport processes that occur across spatial scales, from the chloroplast to the atmosphere (Werner et al., 2012). Knowledge of how the isotopic composition changes under non-steady temporal situations such as the passage of clouds or rapid events of entrainment can enable us to improve the understanding and representation of how the heat, moisture and carbon surface fluxes vary under these conditions (Van Kesteren et al., 2013; Pedruzo-Bagazgoitia et al., 2017).

Our approach combines state-of-the art field measurements with a conceptual model that is specifically designed to support the interpretation of observations. New instrumental developments are enabling measurements of the isotopologues and the isofluxes to be made, in particular for $^{13}\text{CO}_2$ and C^{18}OO (Lee et al., 2009; Sturm et al., 2012; Wehr et al., 2013; Griffis, 2013) at sub-daily scales. We aim to integrate these measurements, normally taken near the surface, in order to identify how local and non-local processes determine the diurnal variability of the isotopic compositions. To this end, we analyse a four day period measured by Wehr et al. (2013) above the Harvard Forest (Wofsy et al., 1993). The comprehensive data set includes the most relevant meteorological variables and stable isotopologues including the turbulent fluxes with a sub-hourly frequency, which are key features of our integrative approach.

Taking the atmospheric boundary layer as the integrating layer between processes occurring at the surface and free atmosphere conditions, we design and test a biochemically and physically sound modelling framework that integrates the essential surface and upper atmospheric biochemical and physical processes occurring at the sub-daily scale. The model solves the governing equations of the CO_2 and H_2O isotopologues for the mole fraction as conserved variables, including their exchange fluxes, coupled to the dynamics of an atmospheric convective boundary layer. Our model parameterizations of the isotopologues are based on the seminal work by Lee et al. (2009), henceforth called L2009, and Lee et al. (2012). Our method aims to study this coupled system using a conceptual, yet realistic, soil-vegetation-atmospheric model (Vilà-Guerau de Arellano et al., 2015).

In developing this modelling framework, and inspired by Baldocchi and Bowling (2003), we create a model framework that will enable us to generate and test hypotheses and interpret field observations. More specifically, to be able to analyze how the net ecosystem exchange depends on the contributions by plants and soil processes. Within the myriad of linkage processes occurring at the different scales, we select one local and one non-local process, to demonstrate the possibilities of our model framework combined with detailed observations. The first is related to the study of how a representation that includes the diurnal variability at the leaf level of the water-carbon isotopic composition, can improve the interpretation of the C^{18}OO isoflux compare with representations that assume steady-state conditions (Yakir and Sternberg, 2000). The second aims to show whether surface measurements of the stable isotopologues are sensitive to rapid entrainment of air masses, the so-called dry tongues (Couveaux et al., 2006), potentially characterized by different isotopic composition originated at the residual layer. By discussing these examples, we extend the work by Lee et al. (2012) and show the potential of isotopic composition (delta) and isoflux measurements to discriminate local from non-local processes.

The paper is structured as follows. A complete description of the fundamental concepts, model governing equations and parameterization derivations, is given in Section 2. Three Appendices complete this section with the definitions and derivations used in the model formulation. The case description, using both observations and model results, is presented in Section 3 and it shows, as a proof of concept, the usefulness of the model in reproducing the essentials of the land-

atmosphere system. The diurnal variability of the stable isotopologues and their exchange fluxes is discussed in Section 4, where we include an alternative description, more experimentally based, for the isoflux of C^{18}OO . We finalise with a study that quantifies the sensitivity of “virtual” measurements to the entrainment of residual-layer air (Section 5). The conclusions summarise the main findings related to the main goals described above.

2. Modelling the atmospheric isotopologue budget

2.1. Approach

Our approach is based on including the essential processes that determine the evolution of the stable isotopologues of carbon dioxide and water vapor during the ABL diurnal evolution. Under convective cloudless conditions, mixed-layer theory (Lilly, 1968; Tennekes and Driedonks, 1981) has proved useful to study how atmospheric state variables and constituents vary with time (Vilà-Guerau de Arellano et al., 2015).

The fundamental concept is that under convective conditions the ABL dynamics are governed by horizontally averaged 0-dimensional slab equations: one equation for the time evolution of the slab variable and another equation for the difference between the residual layer/ free tropospheric value and the slab value, i.e. the jump at the interface between residual layer and ABL. The ABL dynamics are governed by the mixed-layer equations of the potential temperature (heat), specific humidity (moisture) and the two wind components (momentum). In addition, there is an equation that governs the boundary layer growth.

For conserved variables (potential temperature, specific humidity and atmospheric constituents such as the stable isotopologues expressed in mixing ratio), mixed-layer theory assumes well-mixed conditions and a linear variation with height of the turbulent fluxes in the entire ABL. Consequently, variations in time depend solely on the surface and entrainment turbulent fluxes, and on the horizontal advection. The latter acts as a large-scale forcing. Here, we stress that in all the governing equation calculations the mean and fluxes are in SI to ensure that they are conserved to diabatic processes.

Under these conditions, the equation that governs the diurnal variability of the stable isotopologues of carbon dioxide and water vapour reads:

$$\frac{\partial \langle c_i \rangle}{\partial t} = \frac{1}{h} [(\overline{w'c'_i})_s - (\overline{w'c'_i})_e] - \text{Adv}(c_i). \quad (1)$$

where c_i is the generic stable isotopologue, in our case CO_2 , $^{13}\text{CO}_2$, C^{18}OO , H_2O and H_2^{18}O , in mixing ratio units. A key concept of mixed-layer theory is the definition of a slab variable that characterizes the state thermodynamic and atmospheric compound variables over the entire ABL. Profile observations of the potential temperature, specific humidity and CO_2 have shown that the assumption of well-mixed conditions is fulfilled from the surface until the entrainment zone during daytime convective diurnal conditions Vilà-Guerau de Arellano et al. (2004). The mixed-layer variable $\langle c_i \rangle$ is defined as the integral of the stable isotope profile $c_i(z)$ in the entire boundary layer, from the roughness length z_0 until the boundary layer height h . This definition reads:

$$\langle c_i \rangle = \frac{1}{h - z_0} \int_{z_0}^h \overline{c_i(z)} dz. \quad (2)$$

The $(\overline{w'c'_i})_s$ and $(\overline{w'c'_i})_e$ represent the surface and entrainment turbulent fluxes, respectively, connected linearly. Our flux sign convention is positive (negative) flux increases (decrease) the stable isotopologue within the ABL. Fig. 1 visualizes Eq. (1) by showing the mixing ratio and flux profiles and their connection with the vegetation and soil. Note that the contribution due to the horizontal transport ($\text{Adv}(c_i)$) is included in Eq. (1), but not in Fig. (1). If necessary, this advective term can enter in the numerical experiments as a large scale forcing. A

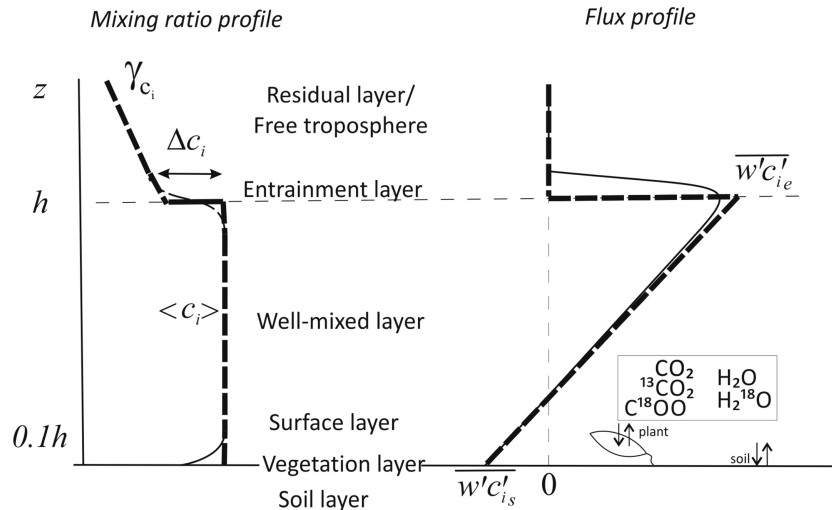


Fig. 1. Main processes governing the diurnal evolution of each stable isotopologue in an interactive atmosphere-land system. Surface flux exchanges ($(\bar{w}'c'_i)_s$) depend on the vegetation conditions (represented by the A-gs model and soil efflux). For the turbulent fluxes, a negative sign indicates an uptake of the compound c_i from the ABL by the plant or soil. In the mixed-layer, the mean profile (left) is constant with height and the flux profile is linear (right). The thin continuous lines indicate more realistic profile and the thick dashed line the profiles after mixed-layer assumptions are applied. The flux exchange at the interface between the residual layer/free tropospheric and the atmospheric boundary layer is represented by an entrainment flux ($(\bar{w}'c'_i)_e$). In the mixed-layer model this entrainment flux is parameterized as a product of the ABL growth rate (entrainment velocity) and the stable isotope jump (Δc_i). This jump depends on the lapse rate (γ_{c_i} in the residual or free tropospheric layers). Note that large scale forcings like advection ($Adv(c_i)$) and mean vertical velocity subsidence influencing h are not included in the figure, but they can be prescribed in the numerical experiments.

complete description of the surface and atmospheric dynamic models can be found in van Heerwaarden et al. (2010) and Vilà-Guerau de Arellano et al. (2015), with an extension to atmospheric compounds (Vinuesa and Vilà-Guerau de Arellano, 2003; Ouwersloot et al., 2012; Janssen et al., 2012). Below we give a short explanation on how we model the surface and ABL dynamics (Section 2.2); and introduce in more detail the new model surface and ABL components to represent the fluxes and mean state of the stable isotopologues (Section 2.3). Note that all the formulation is based on conserved variables. However in comparing with observations, we use the delta notation for each specific isotope in the ABL: $^{13}\text{CO}_2$ (δ_a^{13}), C^{18}OO (δ_a^{18}) and H_2^{18}O (δ_{wa}^{18}).

2.2. State variables: surface and ABL representation

To solve the diurnal evolution for the conserved state variables; wind, potential temperature and specific humidity, we need to prescribe the initial conditions at sunrise (profiles of state variables and atmospheric compounds), and surface/free tropospheric conditions (see Table C.1). We introduce the main components of the land-atmosphere model by the following order: radiation, surface and boundary-layer dynamics. They are:

- 1 Radiation energy balance: the incoming shortwave radiation is calculated as a function of the latitude, longitude and time of the year. The outgoing shortwave radiation depends on the surface albedo. The incoming and outgoing longwave radiation are based on the Stefan-Boltzmann law and therefore depend on the temperature and emissivity. For the outgoing longwave component, we use a surface (skin) temperature. The incoming longwave radiation depends on the temperature at the top of the atmospheric surface layer. This atmospheric surface layer is defined as a 10% of the boundary layer height.
- 2 Surface energy balance: we follow the formulation described at van Heerwaarden et al. (2010). The surface fluxes are represented by an aerodynamic resistance (for both sensible and latent heat fluxes), inversely proportional to the wind, and a canopy resistance. The latent heat flux is composed by a soil, vegetation and dew component depending on the vegetation fraction. The dependencies of

evapotranspiration on radiation and thermodynamic contributions follow the Penman-Monteith equation. The ground flux is calculated with a force-restore model represented by two-soil layers.

- 3 Leaf and canopy dynamics: the water and carbon exchange (plant transpiration and CO_2 assimilation) as part of the surface energy balance model are represented by a two-big leaves model. This model represents photosynthesis at leaf level (A) and the stomatal conductance (gs), i.e. A-gs model. It accounts for the effects of sunlit and shaded on the canopy and the atmospheric temperature (Jacobs and de Bruin, 1997; Pedruzo-Bagazgoitia et al., 2017). The exchange at leaf scale depends on an internal leaf carbon dioxide concentration c_{leaf} , depending on the water vapour deficit, and a leaf conductance. Upscaling to the canopy level depends on the density of vegetation (leaf area) over a given surface ground area, i.e. the canopy surface resistance depends on the leaf area index (LAI).
- 4 CO_2 soil respiration: it is represented by an expression that depends on the soil temperature in the first layer and a soil moisture water stress function. When added to the CO_2 plant assimilation forms the net ecosystem exchange (NEE). The expression is given in A (Eqs. (A.22 and A.23)).

- 5 Atmospheric surface layer: the connection between the fluxes at the surface and the mixed-layer variables is done at the atmospheric surface layer. We follow Monin-Obukhov Similarity Theory to calculate and connect the surface fluxes with the atmospheric variables.

- 6 ABL dynamics: they are governed by the mixed layer equations for potential temperature, specific humidity and wind as well as the boundary-layer height evolution (Lilly, 1968; Tennekes and Driedonks, 1981). The well-mixed assumptions of the atmospheric variables imply a constant profile with height (mixed-layer value) and a linear flux gradient in the ABL (Fig. 1), i.e quasi-steady-state approximation.

To close this set of equations, the buoyancy flux at the entrainment zone is set to 20% of the surface buoyancy flux. Under the presence of shear at the surface and at the entrainment zone, this value becomes higher (Conzemius and Fedorovich, 2006). For all the state variables and atmospheric constituents, the entrainment zone is characterized by an infinitesimal thickness and it is governed by an

entrainment velocity (depending on the boundary layer growth and subsidence) and the difference between the free tropospheric value and the mixed-layer value, i.e. zero-order jump.

2.3. Isotopologues: surface and entrainment flux representation

Eq. (1) shows that the diurnal variability of any atmospheric constituent depends on the surface and entrainment flux. Focusing on the stable isotopologues, in our modelling framework, we relate the surface turbulent flux of the heavy isotopologue to the light and abundant one. As derived in Section A (Eq. (A.15)), the turbulent flux $(\bar{w'}c'_i)_s$ of the isotopologue c_i expression reads:

$$(\bar{w'}c'_i)_s = \frac{\langle c_i \rangle}{\langle c \rangle} (\bar{w'}c')_s + R_{\text{ref}} \langle c \rangle \bar{w'}\delta'. \quad (3)$$

where, from now on, c represents the most abundant and light isotopologue, either CO_2 or H_2O (calculated through the specific humidity q) and $\langle c_i \rangle$ is the less abundant and heavier isotopologue. Eq. (3) shows that of $(\bar{w'}c'_i)_s$ depends on the turbulent flux of the abundant isotopologue $(\bar{w'}c')_s$ (first term right hand side) and the fractionation processes represented by the isoflux $(\bar{w'}\delta')$ (second term) at the surface as proposed by L2009. R_{ref} is the heavy-to-light isotope of the VSMOW standard for oxygen and of the VPDB standard for carbon isotopes. In Section A, we provide the complete derivation of Eq. (3) following two different approaches, see A.1 and A.2. Their equivalence is shown in A.3.

It is important to stress that Eq. (3) depends on the formulations for the soil and plant exchanges of the specific isotopologues. In consequence, the first term on the right hand side is parameterized according to the soil and plant flux formulations for carbon dioxide and water evapotranspiration. In other words, the net ecosystem exchange $\bar{w'}c'$ (for the isotopologues $^{12}\text{CO}_2$) or the total net evapotranspiration (for H_2O) is defined as

$$(\bar{w'}c')_s = (\bar{w'}c')_{\text{plant}} + (\bar{w'}c')_{\text{soil}} \quad (4)$$

As Fig. (1) and Eq. (1) indicate the other relevant vertical turbulent flux that determines the diurnal variability of the isotopologues is the entrainment flux $(\bar{w'}c'_i)_e$. This flux represents the exchange of air between the ABL and the residual and free tropospheric layers. We parameterize it as follows:

$$\begin{cases} (\bar{w'}c'_i)_e = -\Delta c_i \left(\frac{\partial h}{\partial t} - w_s \right) \\ \frac{\partial \Delta c_i}{\partial t} = \gamma_{c_i} \left(\frac{\partial h}{\partial t} - w_s \right) - \frac{\partial \langle c_i \rangle}{\partial t}, \end{cases} \quad (5)$$

in which Δc_i is the difference between the mixing ratio value of the isotopologue at the free troposphere (c_i^{FT}) and the mixed-layer value $\langle c_i \rangle$ (see mean profile in Fig. (1)). The lapse rate γ_{c_i} represents the variation of height of the isotopologue in the residual or free tropospheric layers. w_s is the subsidence velocity that represents the mean vertical velocity variations with height governed by synoptic dynamics.

2.4. Design and evaluation of the numerical experiment

The numerical experiment is designed to reproduce four successive days observed at Harvard Forest Environmental Measurements Site (HF) in Petersham Massachusetts, USA (42.53°N , 72.17°W). The corresponding days are 16–19 September 2011. The 30-metre tower is located at an old-growth temperate forest mainly composed of red oak and red maple. More information on the site and the research activities can be found at Wofsy et al. (1993) and Moore et al. (1996) and the observations can be downloaded at <http://harvardforest.fas.harvard.edu/data-archive>. The observations include the following variables: radiation (shortwave, longwave and photosynthetically active fluxes), turbulent fluxes (sensible, latent and CO_2 net ecosystem exchange),

state variables (potential temperature, specific humidity and wind) as well as isotopic data of carbon dioxide and water vapor (Wehr et al., 2013). In addition to the observations for the abundant stable isotopes, the isotopic composition and the isofluxes of the isotopologues $^{13}\text{CO}_2$ and C^{18}O enable us to evaluate the sub-daily evaluation of the fractionation. The four successive days are aggregated and mean and standard deviations are calculated to represent the associated averaged characteristics and their diurnal variability. In Section C, Table C.1 summarizes the atmospheric initial conditions for the state variables and the isotopologues.

To compare with the isofluxes measurements, the calculated isotopologue fluxes are multiplied by the mixed-layer CO_2 mixing ratio, following Wehr et al. (2013). Here, we therefore assume as a first approximation that the measurements above canopy are representative for the ABL CO_2 values. The calculated turbulent fluxes, i.e. isofluxes, used in the evaluation against the observations therefore read:

$$F = \langle c \rangle (\bar{w'}\delta'). \quad (6)$$

These calculated fluxes will be compared with the storage and eddy fluxes measured by Wehr et al. (2013). To facilitate the comparison with the observations, we follow here the units and notation given by Wehr et al. (2013). The units are therefore % $\mu\text{mol m}^{-2} \text{s}^{-1}$.

2.5. Mass balance in terms of δ

The specific diurnal contribution of the soil, plant and entrainment processes to the isotopic composition in the ABL expressed in terms of δ is quantified by the mass balance or budget equation. To this end, we derive a budget equation and present the full derivation in A.5. The generic budget equation for the stable isotopologues reads:

$$\frac{\partial \delta_a}{\partial t} = \frac{\bar{w'}\delta'}{h} + \left(\frac{1}{h} \frac{\partial h}{\partial t} \right) \left(\frac{c^{\text{FT}}}{\langle c \rangle} \right) \left(\delta^{\text{FT}} - \delta^a \right) \quad (7)$$

the *surface* terms 1st right hand side represents the various soil and plant fractionation and in consequence depends on the specific isotope. The *entrainment* term includes a dependence on the ABL-dynamics, the entrainment velocity or $\frac{\partial h}{\partial t}$ and the evolution of the isotopologue jump at the interface between the residual layer and the ABL, i.e. $(\delta^{\text{FT}} - \delta^a)$. For the sake of simplicity, the subsidence velocity w_s at Eq. (5) is omitted from the expression, but it can be included in the formulation (Vilà-Guerau de Arellano et al., 2015).

3. Evolution of the atmosphere-land diurnal interaction over the Harvard Forest

Fig. 2 shows the observed and modelled main components of the radiation and surface energy balance above the canopy for the four-days measurement period above the Harvard Forest (Section 2.4). The diurnal amplitude of the net available radiation (Q_n) and the photosynthetic active radiation (PAR) compare satisfactorily as well as the maximum levels of both radiative fluxes (Fig. 2a). After 13 LT the modelled fluxes are higher than observations, probably due to the presence of scatter boundary layer clouds, i.e. cloud cover less than 20% that leads to a slight decrease of the incoming shortwave radiation. It is important to stress that we parameterize PAR in a simple manner by assuming that PAR is 0.5 of the incoming shortwave radiation (Ronda et al., 2001). As Fig. 2a corroborates, in spite of the simplicity of the parameterization, there is good agreement between observations and model results.

In partitioning the available energy, we find that both the calculated sensible heat (SH, Fig. 2b) and latent heat (LE, Fig. 2c) fluxes are slightly underestimated during the morning transition (until 10.30 LT), and overestimated after this time. The disagreement is likely due to modelling assumptions and/or the treatment in inferring the observed fluxes using the eddy-covariance method. For the former, note that the

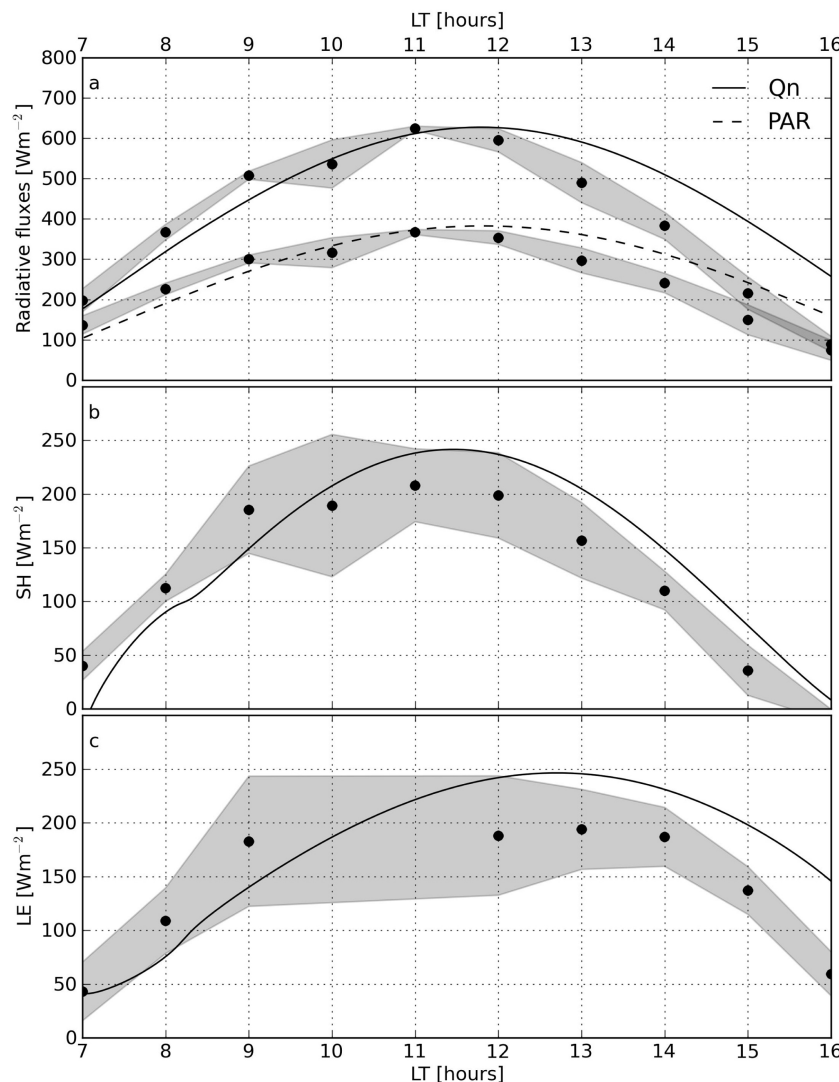


Fig. 2. Diurnal evolution of the (a) net available energy and photosynthetic active radiation, (b) sensible and (c) latent heat fluxes. The observations are aggregated of four consecutive days under similar conditions (16–19th September 2011). Averaged values are shown as dots and the shaded region represents the standard deviations. MXL results are expressed by continuous and dashed lines. Observations were taken above the canopy, at 27.9 m above ground level. For LE, the observations at 10 and 11 LT were missing for the four successive days.

dynamic/thermal canopy effects are omitted. The vegetated canopy is represented by a bulk layer with a dynamic active vegetation using a two-big leaves model that accounts for shaded and sunlit leaves (Pedruzo-Bagazgoitia et al., 2017). Soil dynamics are modelled by a force-restore soil model discretized by two soil layers that depend on soil temperature and moisture, and a skin conductivity. With respect to the observations, it is known that normally the net available radiation and the ground flux are larger than the combined sensible and latent heat fluxes. This imbalance in the surface energy is due to several reasons: omission of the low frequencies in the retrieved turbulent fluxes, canopy effects or secondary circulations triggered by small scale surface heterogeneities (Foken, 2008; Leuning et al., 2018). In analyzing the performance of the evolution of the dynamics of the boundary layer, we will take the non-closure of the surface energy into account.

The evolution of the modelled mixed-layer potential temperature (θ) (Fig. 3a) and specific humidity (q) (Fig. 3b) compared with the four-successive day composite shows the ability of the model to reproduce the diurnal variability with the calculated sensible and latent heat fluxes. As θ and q are governed by an equation analogous to Eq. (1), diurnal variability depends on the surface fluxes, but also on the fluxes

at the ABL top. Consequently, it is crucial to represent the boundary-layer depth (ABL) evolution adequately because entrainment and dilution also influences the diurnal variability of the isotopologues.

Fig. 3c shows the ABL-height evolution, which indicates that once the inversion is broken after 8 LT, there is an initial period in which entrainment is dominant due to the ABL rapid growth (until 11 LT) and a more slow growth after this time. To determine the reliability of our ABL-height calculation, we have evaluated the ABL calculation by comparing with the radiosounding taken at Albany (42.70°N, 73.83°W) at 00 UTC (19 LT). From the weather balloon profiles, we estimate the ABL height as the level in which the maximum gradient in potential temperature is found. We also inferred this height based on a composite of the four-successive day weather balloon measurements. The aggregated observation results in an ABL height of 2045 m with a standard deviation of 100 m. As shown in Fig. 3c this observed value corresponds well with the modelled value at 15 LT that is already representative for the late afternoon boundary layer, and in consequence it can be roughly compared with the 19 LT observation. Note that this value integrates the ABL dynamics influenced by the morning transition, period dominated by entrainment, and the more slow ABL development after 12 LT.

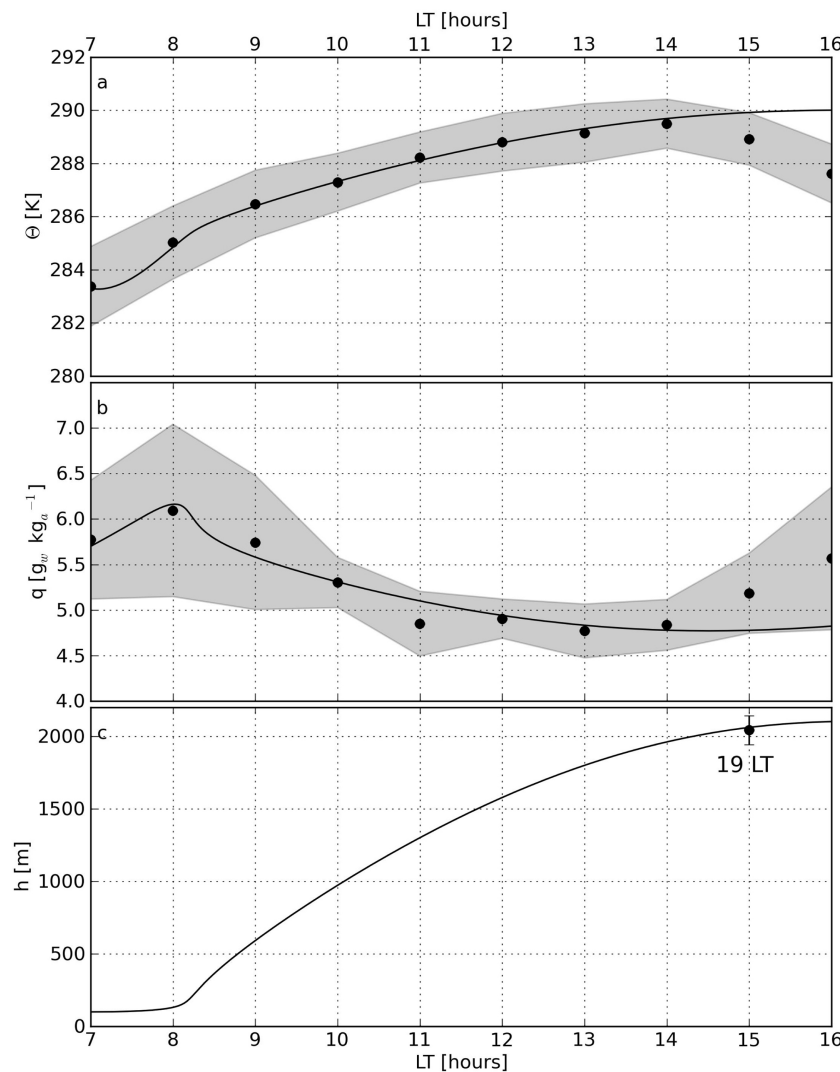


Fig. 3. Diurnal evolution of (a) potential temperature, (b) specific humidity and (c) boundary layer height. Treatment of observations and model results similar to Fig. 2. In (c) an observation of the boundary layer height inferred from four weather balloons launched at Albany at 00 UTC (19 LT) is included for comparison with boundary layer height results.

As Fig. 3a and b show, the mixed-layer potential temperature and specific humidity modelled are in close agreement with the observations. Specific features such as the maximum of the specific humidity at 8 LT due to the moistening of the shallow boundary layer before the break up of the ground inversion after 8 LT are well reproduced. The diurnal evolution after this time shows that the overestimation in the modelled evapotranspiration flux above the canopy is compensated by the drying entrainment. Note that in absence of θ - and q -observation profiles in the residual layer and free troposphere, we impose values for the initial jumps of potential temperature and of the specific humidity as well as their respective lapse rate in the free troposphere constrained by the temporal evolution of θ and q .

4. Diurnal carbon cycle: light and heavy isotopic composition

4.1. Mixing ratio and isotopic composition evolution

The diurnal mixing ratio evolution for the total carbon dioxide and the isotopic composition for carbon ($\delta_a^{13}\text{C}$) and oxygen ($\delta_a^{18}\text{O}$) are shown in Fig. 4. The CO₂ diurnal pattern is characterized by a large decrease between 7 and 9 LT (7.0 ppm h⁻¹) and a more steady decrease in the subsequent hours. This decrease during the morning transition is mainly driven by plant assimilation (see NEE in Fig. 5) and thereafter 8

LT by entrainment of air masses characterized by lower mixing ratio from the residual layer (Vilà-Guerau de Arellano et al., 2004). In the first two hours the disagreement between model and observation is larger in spite of the fact that the model satisfactorily reproduces the NEE observations (see in Fig. (5 a)). Two processes that are not explicitly taken in our numerical experiment setting conditions into account can possibly explain this disagreement. The first one is horizontal advection of the carbon dioxide isotopologues. The second one is related to the interaction between the canopy and atmosphere during the night and morning transition. During the night the ecosystem respiration leads to an increase of isotopic depleted CO₂. The advent of turbulence driven by the positive values of the sensible heat flux leads to the transport of the isotopologues by canopy venting driven by sweeping and ejection motions at the interface canopy-atmosphere. Both contributions can be prescribed, but in the present numerical experiments assumptions are kept to a minimum.

After 9 LT the agreement between CO₂ model results and observations is very satisfactory indicating a balance between the assimilation flux at the surface, the ¹²CO₂ soil efflux and the entrainment flux at the ABL top. With respect to the last, it is important to stress that here in absence of upper atmospheric isotopologue observations, we constrain the jump of CO₂, ¹³CO₂ and C¹⁸OO at the entrainment zone (Δc and Δc_i , see Fig. 1) with residual layer values for the three isotopologues that

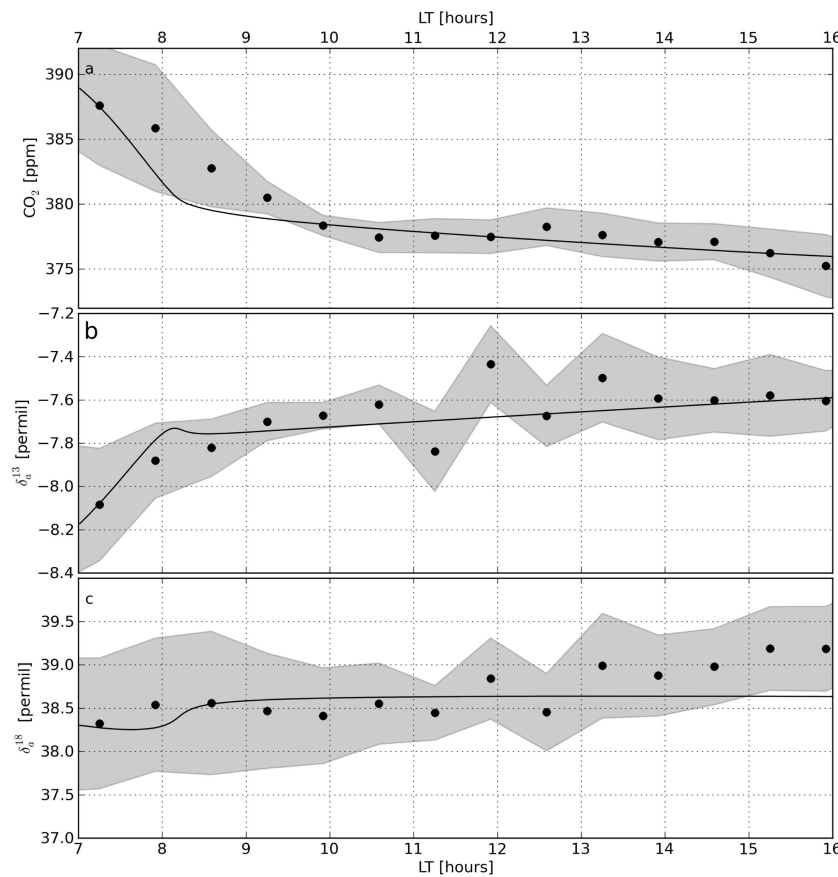


Fig. 4. Diurnal evolution of the (a) CO_2 , (b) δ_a^{13} and (c) δ_a^{18} . Treatment of observations and model results similar to Fig. 2.

lead to the best agreement with observations. As Table C.1 indicates, we prescribe morning initial negative jumps of the heavy isotopologues at the interface ($\langle c \rangle$ residual layer $<\langle c \rangle$ ABL), closing following the negative jump for CO_2 . This corresponds to higher CO_2 mixing ratio in the ABL due to the respiration by vegetation during the night. The physical interpretation for the isotopic composition is as follows: night respiration leads to a higher value of δ_a^{13} in the nocturnal boundary layer ($-7.88\text{\textperthousand}$) with respect to the values at the residual layer ($-8.17\text{\textperthousand}$). In other words, this initial value of Δc_t carries information on the differences on the isotopic composition between soil and plant processes in direct contact with the surface, *i.e.* the nocturnal boundary layer, and the residual layer above which is uncoupled from the surface.

The isotopic composition for carbon and oxygen in CO_2 , δ_a^{13} and δ_a^{18} are shown in Fig. 4a and b. For δ_a^{13} and δ_a^{18} the agreement of the control experiment (CTL) with the four-day averaged observational data is very satisfactory with a realistic representation of the morning transition. For δ^{13} , the model is in close agreement with the morning increase from $-8.2\text{\textperthousand}$ until $-7.7\text{\textperthousand}$ from 7 till 8 LT. In the case of δ_a^{18} the morning transition effect is minimal, but also associated with an increase until the ABL begins to grow. Specific humidity is the meteorological variable shows a similar behaviour. The maximum at around 8 LT (Fig. 3b) marks the start of the boundary layer growth associated with the processes of entrainment and dilution.

The correct representation of the plant and soil surface fluxes is crucial in order in Eq. (4) to reproduce the isotopologue diurnal variability. Fig. 5a demonstrates satisfactory agreement between the model calculation and the observations of NEE flux for CO_2 . The modelled NEE calculation is within the range of the four day variability and it reproduces the maximum uptake values between 10 and 12 LT as well as the diurnal amplitude. Relevant for our study is that the observed storage flux is negligible compared to NEE. This provides further support of our assumption to treat the canopy as a bulk representation

using a two big-leaves model for the vegetation and a force-restore soil model. We are aware that important processes occurring in and above the canopy-atmosphere interface are oversimplified, but in this study our aim is to reproduce the variability of the isotopic composition of CO_2 and H_2O related to the ABL dynamics at the sub-diurnal scale and the essential interactions between the atmosphere, vegetation and soil processes above the canopy.

NEE calculation relies on the separate representation of the CO_2 exchanges between the atmosphere and the soil and plant processes (Fig. 5b). The CO_2 plant assimilation representation, *i.e.* A-gs model, includes the leaf and the canopy scale. At the leaf scale, the dependence of the stomatal aperture on PAR radiation and on the atmospheric temperature and vapour pressure deficit (Ronda et al., 2001) requires a reliable representation of these variables as shown by Figs. 2a, and 3 a and b, respectively. In addition, and since assimilation depends on the gradient between the CO_2 atmospheric mixing ratio and the internal leaf concentration ($\text{CO}_{2\text{leaf}}$), the temporal variability of these variables needs to be accurately modelled (see Figs. 4a and 7 a). In upscaling to the canopy level, the two-big leaves model implemented here requires an adequate representation of direct and diffuse radiation depending on the leaf area index. The satisfactory agreement with the available Gross Ecosystem Production (GEP), that includes the gross photosynthesis and photorespiration both in the model and observations, ensure us that the model is able to reproduce the order of magnitude and the evolution of the CO_2 canopy assimilation. GEP was calculated from the NEE observations using the method proposed by Reichstein et al. (2005). The good match between observations and model CO_2 efflux (Fig. 5b) ensures us the availability of our model in reproducing the key components of the CO_2 diurnal cycle. Here it is important to model the soil temperature and moisture in order to get a reliable estimation (see Eq. (A.22)). As shown by Fig. 5b the soil efflux has a positive contribution to the CO_2 tendency which can not be neglected since it partly offsets

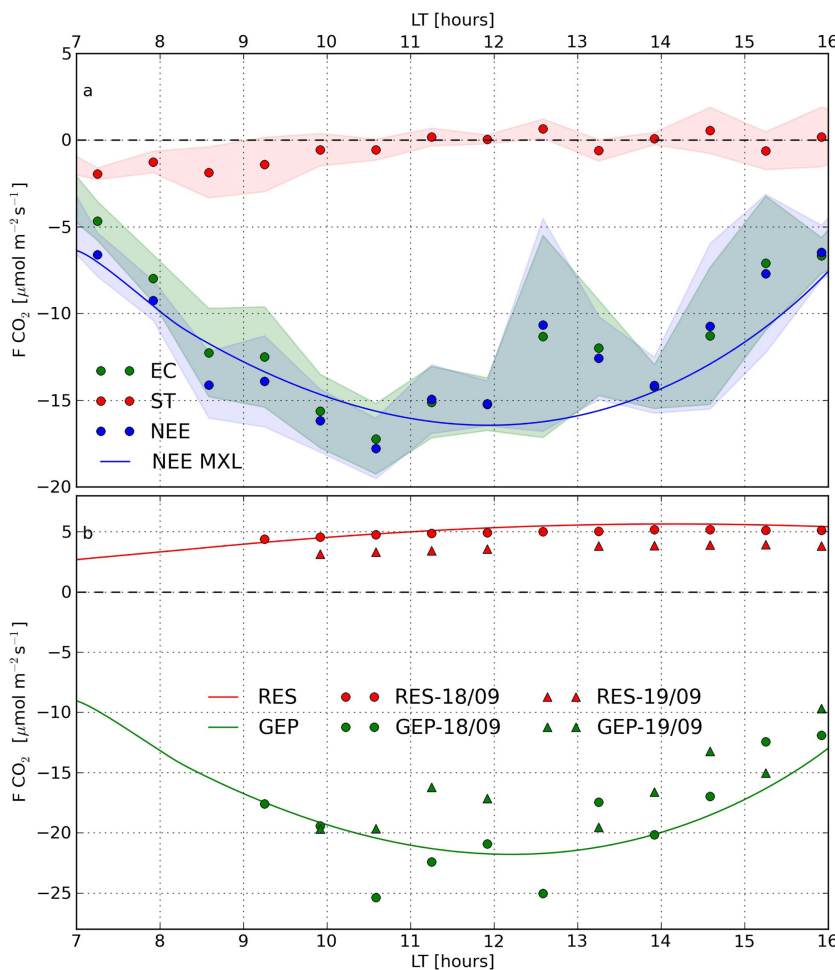


Fig. 5. Diurnal evolution of the CO₂ flux: (a) eddy flux (EC), storage (ST) and net ecosystem exchange (NEE), and (b) the contributions by plant (GEP) and soil respiration (RES) processes. Treatment of observations and model results similar to Fig. 2. For GEP and RES only the 18th and 19th September 2011 measurements were available.

the uptake of carbon dioxide from the atmosphere. The calculated values agree well with the ones reported by Wu and Lee (2011) at the Harvard Forest. For the same location, they reported diurnal measurements slightly below 5 $\mu\text{mol m}^{-2} \text{s}^{-1}$.

Key in the flux representation, it is the calculation of CO₂ in between the soil, plant and atmosphere interface. In particular, the specific representation of C¹⁸O₂ is more complex than ¹³CO₂ in order to account for the isotopic equilibration between water and carbon dioxide within the leaf. Following L2009, we introduce in the formulation a concentration in the chloroplast (CO_{2cs}) and in the soil (CO_{2soil}). These variables are needed in the calculation of the isoflux from the plant (Eq. (A.31)) and soil (Eq. (A.33)). Therefore, to complete the relation between fluxes and gradient concentrations, Fig. 6 shows the sub-diurnal evolution of the following CO₂ mixing ratios: atmospheric, internal leaf, chloroplast and soil, and their ratio with respect to the atmospheric mixed-layer CO₂ mixing ratio (CO_{2atm}). In the A-gs model formulation, the internal leaf concentration depends on the vapour pressure deficit and follows a diurnal variability similar to the one of the mixed-layer atmospheric CO₂. For this case, the ratio CO_{2leaf}/CO_{2atm} is below 0.8, but within the range of observed values (Katul et al., 2000). Fig. 6b shows the internal leaf CO₂ mixing ratio characterized by values lower than the atmospheric CO₂ mixing ratio due to photosynthesis (Flexas et al., 2008). The calculation of the chloroplast CO₂ concentration depends on the mesophyll conductance and the CO_{2leaf} and is based on Eq. (A.32). The ratio of CO_{2cs}/CO_{2atm} is near 0.47, similar to observations reported by Flexas et al. (2008). Note that these values are very

dependent on the species and can vary on long time scales (season) and short time scales (micrometeorology). Following on the analysis of CO_{2cs}, note that this chloroplast concentration depends on the calculation of the mesophyll conductance that is also characterized by a strong diurnal variability. In the modelled case, the values of the mesophyll conductance range from 83 $\text{mmol m}^{-2} \text{s}^{-1}$ (2.1 mm s^{-1} , conversion factor using the ideal gas law,) at sunrise/sunset to maximum values between 12 and 14 LT near 175 $\text{mmol m}^{-2} \text{s}^{-1}$ (4.1 mm s^{-1}). These values are within the range of observations as presented by Flexas et al. (2008).

The CO₂ soil mixing ratio, calculated according Eq. (A.35), shows a large diurnal variability with a minimum of 600 ppm after sunrise and a maximum value of 810 ppm at 16 LT. These values slightly underestimate reported measurements, but they are within the range of observations taken at soil forest of similar characteristics (Risk et al., 2002; Bekele et al., 2007). We are aware of the large spatial variability of CO₂ soil mixing ratios and their dependence on the soil depth, soil temperature and soil moisture, but here we aim to model a representative CO₂ soil concentration for the Harvard forest.

4.2. The evolution of isofluxes

The calculated ¹³CO₂ isoflux as well as the plant and soil contributions are compared against the eddy-covariance and storage isoflux observations in Fig. 7. Note that a positive value of the isoflux indicates an enrichment of the isotopologue in the atmosphere, in that

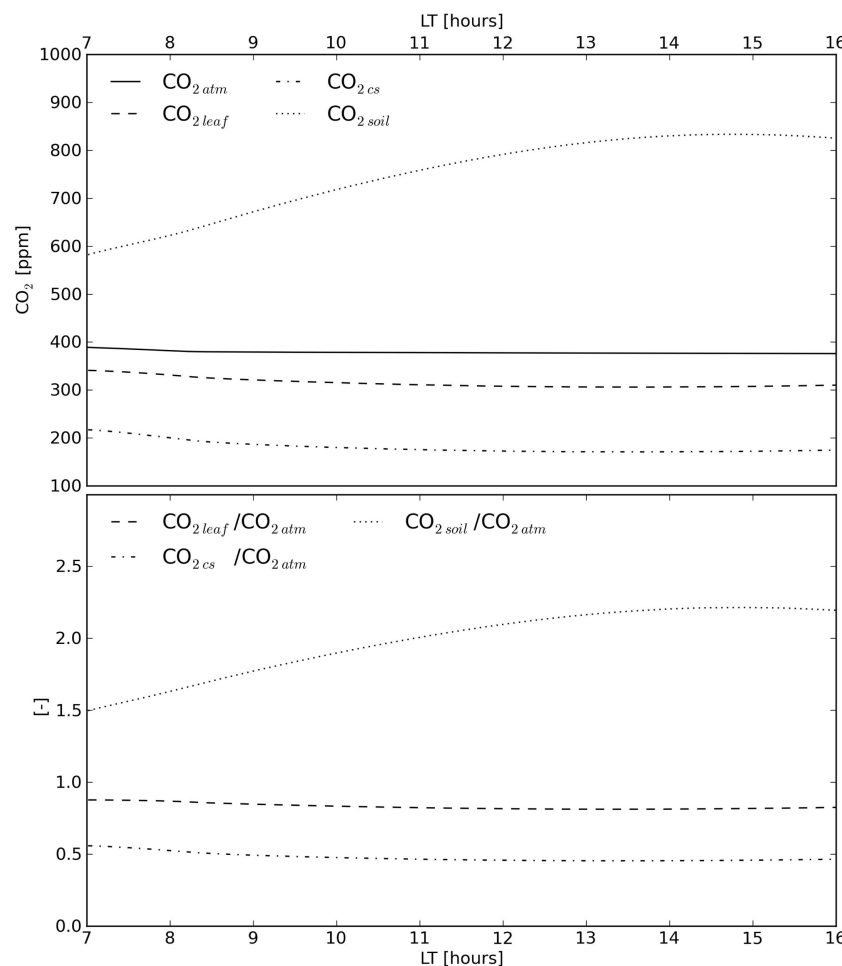


Fig. 6. Diurnal evolution of the CO_2 mixing ratio used in the plant and soil parameterizations: atmospheric mixed-layer, inner leaf (c_{leaf}), mesophyll (c_{cs}) and soil (c_{soil}) (a) and the ratio of the leaf, mesophyll and soil CO_2 with respect to the atmospheric value. Note that the atmospheric CO_2 mixing ratio evolution is the same as the one shown in Fig. 4a.

case $^{13}\text{CO}_2$, with respect to the abundant isotopologue, CO_2 . The agreement of modelled and observed NEE is very satisfactory which indicates that the parameterization combining the plant CO_2 assimilation flux adjusted by the isotopic discrimination (Eq. (A.18)) and the soil isoflux aim to reproduce the diurnal variability as well as the maximum enrichment of the isotopic composition between 11 and 14 LT. Photosynthesis prioritizes the assimilation of $^{12}\text{CO}_2$ relative to $^{13}\text{CO}_2$. The observations present larger fluctuations around this interval, but the calculated evolution is within the positive and negative sub-daily fluctuations. Similar to Fig. 5 the storage term is negligible compared to the eddy-covariance term. Similar to L2009, the canopy-scale kinetic fractionation ϵ_k^{13} (Eq. (A.20)) is almost constant with time and with a value equal to 3.95‰ during the light hours. Fig. 7b corroborates that the NEE diurnal variability follows closely the isoflux plant contribution and that the soil component is relevant (accounts for approximately 20%) but with an almost constant isoflux over time.

Fig. 8a shows the evolution of the observed and modelled isoflux of C^{18}OO and the specific contributions to the isoflux by plant and soil processes (Fig. 8b). For the plant isoflux, we studied the sensitivity of our results to the two representations: PAR1 and PAR2. The most biologically based parameterization is PAR1 (see A.4.2). Here, we follow closely the formulation suggested by L2009 and further tested by chamber-based measurements by Gangi et al. (2015). We propose PAR2 (see B) as a formulation to study the sensitivity of the isoflux of C^{18}OO to the time evolution of the isotopic water within the leaf. In doing so, we show the capability of our model framework to provide guidance to potential improvements of the Craig–Gordon parameterization (PAR1),

and stress the need to test them with a (likely non-steady-state) model that accounts for the coupling the soil, vegetation and atmosphere.

Fig. 8 shows the four-day aggregate measured eddy-covariance (EC) and storage (ST) fluxes as well as NEE compared with the two parameterizations of the isoflux of C^{18}OO . The comparison with the eddy-covariance isoflux shows that PAR2 is able to capture better the diurnal variability and reproduce the change of sign of the isoflux C^{18}OO at 13.5 LT. PAR1 is less sensitive to the diurnal variations and the calculated isoflux oscillates between -120 and around $-60\text{‰ } \mu\text{mol m}^{-2} \text{s}^{-1}$. Compared to PAR2, the C^{18}OO isoflux calculated by PAR1 remains negative throughout the day. This indicates that the two dependences on the meteorological variables, T_c at Eq. ((A.25)) and RH at Eq. ((A.26)), characterized with opposite diurnal variability, are compensating and cancel the effect of diurnal variability on PAR1. Fig. 8b shows that the parameterization of the soil flux is also relevant. The negative values, below $-100\text{‰ } \mu\text{mol m}^{-2} \text{s}^{-1}$, are of similar order as the plant fluxes and it can be determining in the positiveness or negativeness of the net C^{18}OO isoflux. Due to the dependence on the CO_2 soil respiration flux, this result indicate the need to have proper estimation of this flux and the soil CO_2 mixing ratio.

This change of sign also depends on the representations of the plant processes. PAR1 and PAR2 show a shift from depletion to enrichment. For PAR1, it occurs at 8.5 LT whereas for PAR2 the sign changes just before midday. After this transition from depletion to enrichment, PAR1 shows a small amount of diurnal variability compared with the results obtained using PAR2. The impact of the isoflux C^{18}OO on the δ -variability is noticeable by analyzing the δ_a^{18} from 7 LT until 9 LT

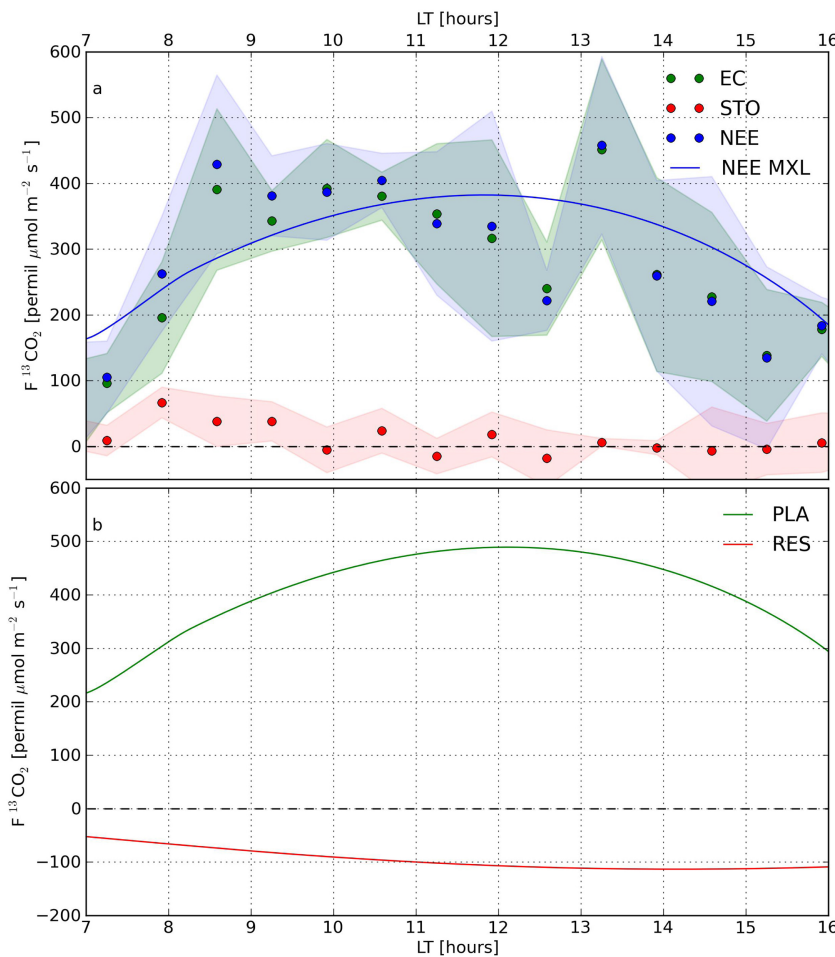


Fig. 7. Diurnal evolution of the $^{13}\text{CO}_2$ isoflux: (a) eddy flux (EC), storage (ST) and net ecosystem exchange (NEE), and (b) the contributions by plant (PLA) and soil respiration (RES) processes. Treatment of observations and model results similar to Fig. 2. Isofluxes are defined according to Eq. (6).

(see Fig. 4). When the entrainment process is more active, the more negative values by using PAR1 results in a slower enrichment at around 8 LT. The relevance of entrainment at this time is quantified later on by analyzing the budget. In discussing these results, it is relevant to stress that for previous measurements taken at Harvard forest, Wehr et al. (2013) observed for an early and more active period, 30th June until 4th July 2011, a similar transition from low negative values, closely following NEE, to high positive values. This positive flux, named by Gillon and Yakir (2001) retroflux, quantifies how the photosynthetic activity regulates the diffusion of C^{18}OO from the leaf to the atmosphere. However, note that other measurements, as reported by L2009 and shown in their Figure 3, only show positive values of the C^{18}OO isoflux during the entire day (observations taken above a soybean canopy).

Our modelling framework enable us to analyze the sub-daily evaluation of key components of the parameterizations PAR1 and PAR2. Fig. 9a shows the two atmospheric variables that drive $\delta_e^{18}\text{O}$ (Eq. (A.25)): the canopy temperature and the relative humidity (included in δ_{lw}) at the surface. The calculated $\delta_e^{18}\text{O}$ (Eq. (A.25)) includes two contributions: δ_{lw} (first r.h.s term) and the second term that depends on the canopy temperature (Fig. 9b). To complete the comparison, we present in Fig. 9c the $\delta_{eff}^{18}\text{O}$, which accounts for the leaf water isotopic composition following the PAR2 formulation in Appendix B. The four-day observed composite and model calculation compare very satisfactorily which corroborates that, both surface and entrainment processes, are well represented for the calculation of the moisture budget. By comparing

Figs. 9b and c, we find that both are characterized by diurnal variability, but with different timing and amplitude of the diurnal maximum values: $\delta_e^{18}\text{O}$ is approximately $\delta_{eff}^{18}\text{O} + 10\%$ and the peak after 12 LT. For $\delta_e^{18}\text{O}$ this variability is due to the first term on the right-hand-side of Eq. (A.25) depending on the relative humidity whereas the term depending on T_c (Brenninkmeijer et al., 1983) remains almost constant with time (2nd term r.h.s Eq. (A.25)). These dependencies on the meteorological variables in Eq. (A.25), i.e. RH and T_c , indicate the need to calculate the isofluxes of C^{18}OO with a fully coupled soil-atmosphere-vegetation model. In absence of plant and meteorological data necessary to apply PAR1, PAR2 offers an alternative by prescribing and calculating $\delta_{eff}^{18}\text{O}$ in Eq. (B.2) in order to take the leaf-water fractionating diurnal variability into account (Cernusak et al., 2002).

4.3. The δ -budget

To quantify more explicitly the contributions of surface and the residual/free troposphere driven atmospheric processes to the diurnal variability of the isotopologues, we calculate each specific term of Eq. (7), i.e. the contributions of the temporal term (tem) (left-hand-side term of the equation), surface (sur, first-right-hand side term) and entrainment (ent, 2nd r.h.s term). For surface, we add the specific contributions of the plant and soil processes. In a similar manner, we derive and calculate the δ -budget following Eq. (7). The complete derivation is presented in the Appendix (A.5).

Fig. 10 shows the temporal variation of the individual terms that

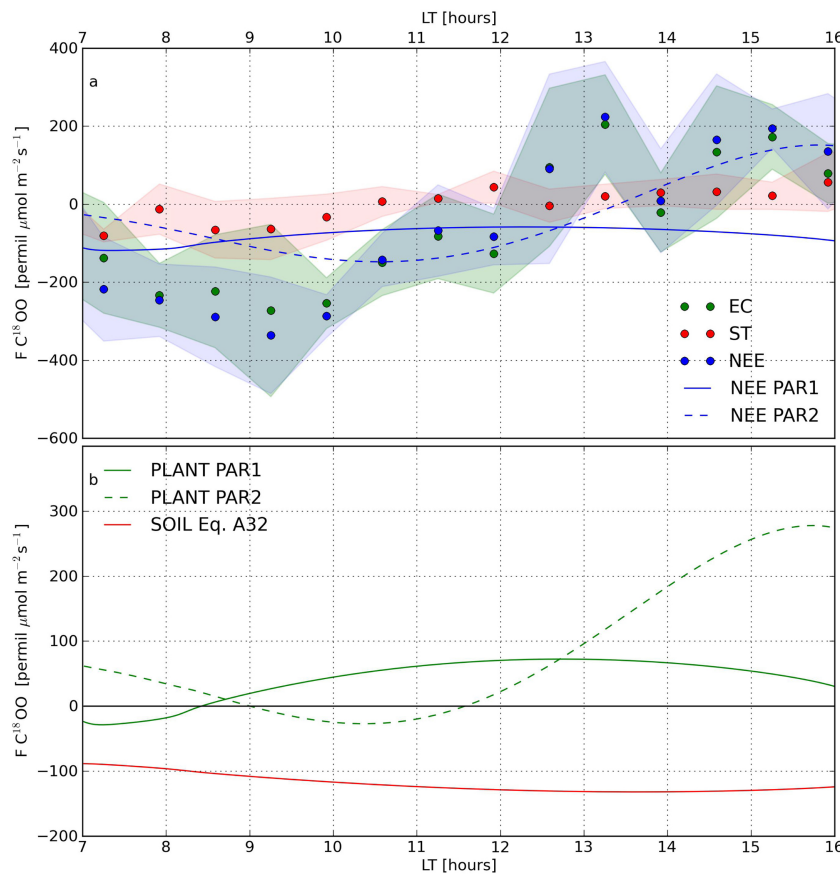


Fig. 8. Diurnal evolution of the $C^{18}OO$ isoflux: (a) eddy flux (EC), storage (ST) and net ecosystem exchange (NEE), and (b) the contributions by plant (PLA) and soil respiration (RES) processes. Treatment of observations and model results similar to Fig. 2. Isofluxes are defined according to Eq. (6).

contribute to the mass budget of δ_a^{13} and δ_a^{18} . Note that the sign of the contribution physically means that positive (negative) values indicate an enrichment (depletion) of $^{13}\text{CO}_2$ in the atmosphere relative to CO_2 . The positive values of the $^{13}\text{CO}_2$ surface plant contribution indicate the preference of photosynthesis in assimilating the abundant isotopologue $^{12}\text{CO}_2$ relative to $^{13}\text{CO}_2$. This enrichment of δ_a^{13} with maximum values of 0.6‰ h^{-1} are partly compensated by the always negative values by soil fractionation processes. To complete the budget, the results show unequivocally that the entrainment process can not be omitted. The δ_a^{13} -budget shows that the air entrained originated at the residual layer is depleted of $^{13}\text{CO}_2$ relative to CO_2 after 7.2 LT. As shown by the inset in Fig. 10 a, the jump $\Delta\delta^{13}$ changes sign at 7.2 from an enrichment to a depletion on the isotopic composition. As such, the entrainment contribution depletes and tends to decrease δ_a^{13} . This entrained air with a different isotopic signature can be physically interpreted as (a) processes occurring in the previous day due to the interaction between the atmosphere and the forest and (b) influence of large-scale transport during the night.

In contrast, the δ_a^{18} budget (Fig. 10b) is different than the δ_a^{13} . Both surface terms driven by plant and soil processes, contribute to a depletion of ^{18}O in CO_2 within the ABL whereas the positive temporal term is mainly driven by the entrainment of air enriched in ^{18}O with a maximum at 8 LT, i.e. compared to $\Delta\delta^{13}$, $\Delta\delta^{18}$ remains negative during the day (not shown). Connecting with Fig. 4c, it shows that these higher values of δ_a^{18} are governed by the entrainment process. Finally, as Fig. 4b and c show, and corroborate it by this budget analysis, the contributions of the net surface and entrainment fluxes become less important after the morning transition. In addition, the fluxes compensate each other and as expressed by Eq. (1) leads to a small variation of the mixing ratio. In consequence, after 9 LT the diurnal variability of δ_a^{13} and δ_a^{18} becomes small, reaching almost an steady-state.

5. Detecting rapid entrainment event by variations on the isotopic signature

The previous section quantified insights into the relevance of local and non-local processes by calculating the δ -budgets. As shown in Fig. 10, entrainment makes a similar contribution to that of the surface processes to controlling the diurnal variability of δ_a^{13} and δ_a^{18} . However, the quantification and representation of this term remains elusive due to the difficulty of measuring it. Here, we discuss a set of three interconnected numerical experiments aimed at determining the responses of the isotopologues and isofluxes to intermittent variations in isotopic composition driven by the entrainment process. These experiments aim to analyse how non-local processes influence isotopic composition and how they can be determined by surface measurements. Assuming the case discussed above to be representative (control, CTL), we disrupt the case CTL conditions after one hour (at 8 LT) to mimic a brief event of air entrainment reaching the surface. The event lasts 200 s. In the course of the subsequent 200 s the CTL conditions are restored. Entrainment events normally last for only a few minutes and they are due to the subsidence of air masses that reach the surface to compensate for the rise of convective turbulent thermals (see Figure 4d in Couvreux et al. (2006)). They are characterized by fluctuations in potential temperature and specific humidity. For the latter, they oscillate between -0.5 g kg^{-1} and 0.5 g kg^{-1} . In the sensitivity experiments that we propose, the entrainment of air from the residual layer modifies the specific humidity on the $\langle q \rangle$ -mixed-layer value, but more importantly they are characterized by a different conditions in the isotopic composition.

We first explain the three experiments: in the first, which mimics only entrainment of dry air (EDA), we study how a tongue of dry air originating at the residual layer characterized by a lighter content of the

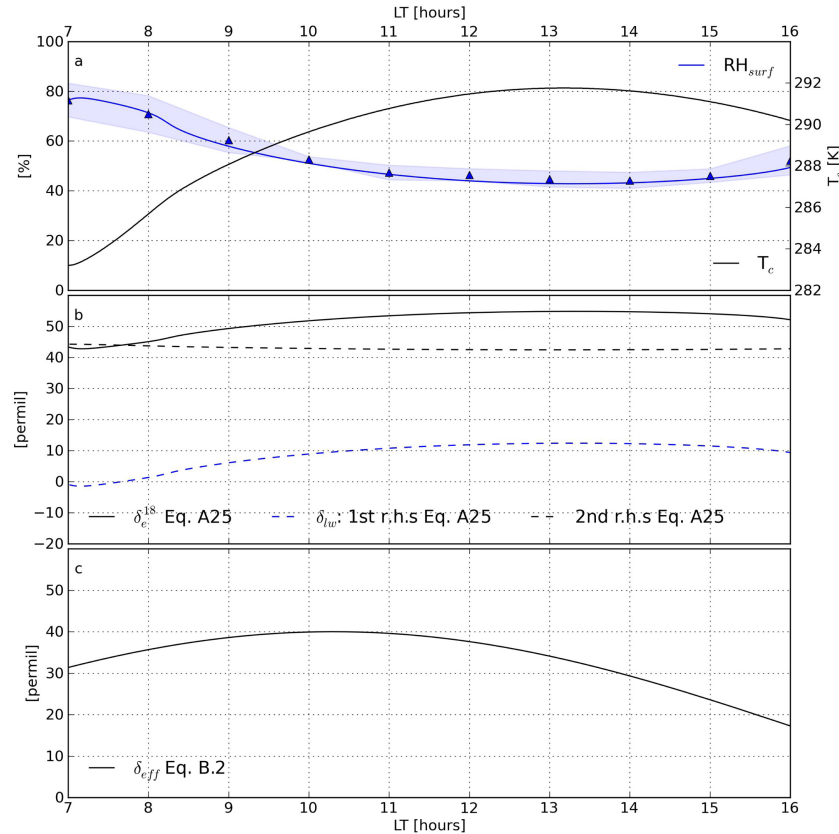


Fig. 9. Diurnal variation (a) of the modelled relative humidity (RH) and canopy temperature (T_c). The observed four-day aggregated values of RH are also shown as they partly determine the dependence on δ_e^{18} (b) of the equilibrium isotopic composition of CO₂ with the water at the evaporation site δ_e^{18} assuming a balance between CO₂ and leaf water calculated according to Eq. (A.25), including the two individual components of the right hand side (r.h.s) equation. (c) the effective δ_{eff}^{18} parameterized according to Eq. (B.2).

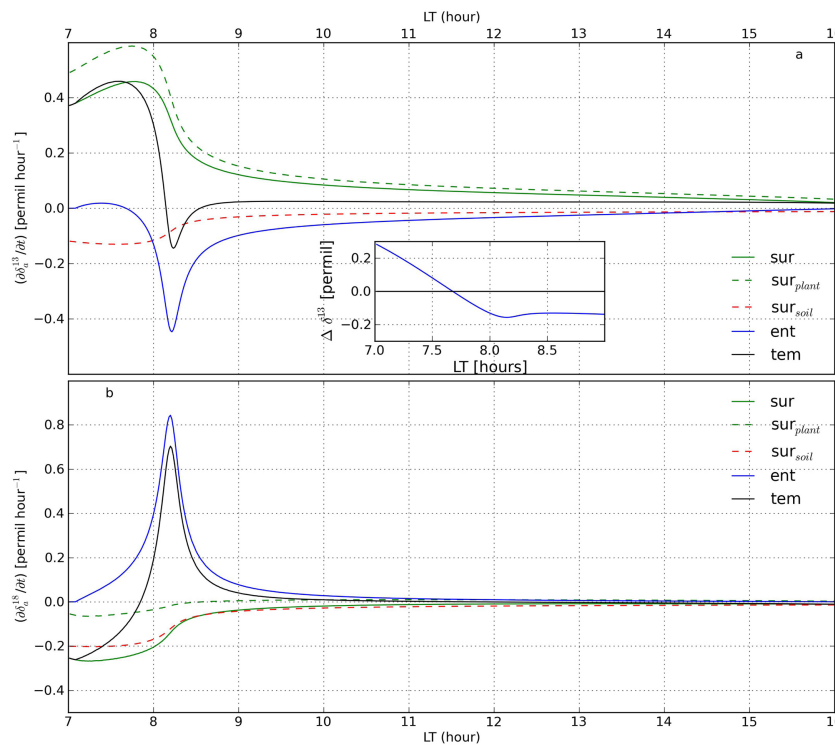


Fig. 10. Diurnal evolution of the contributions of the individual components of the total budget: (a) δ^{13} according to Eq. (7) and (b) δ^{18} . tem is the temporal term, surf is the surface contribution including the individual contributions by plants and soil processes and ent is the entrainment term. The inset figure in (a) shows the change of the sign of the $\Delta\delta^{13}$ defined as the difference on the isotopic signature of δ_d^{13} in the free troposphere and the mixed-layer value.

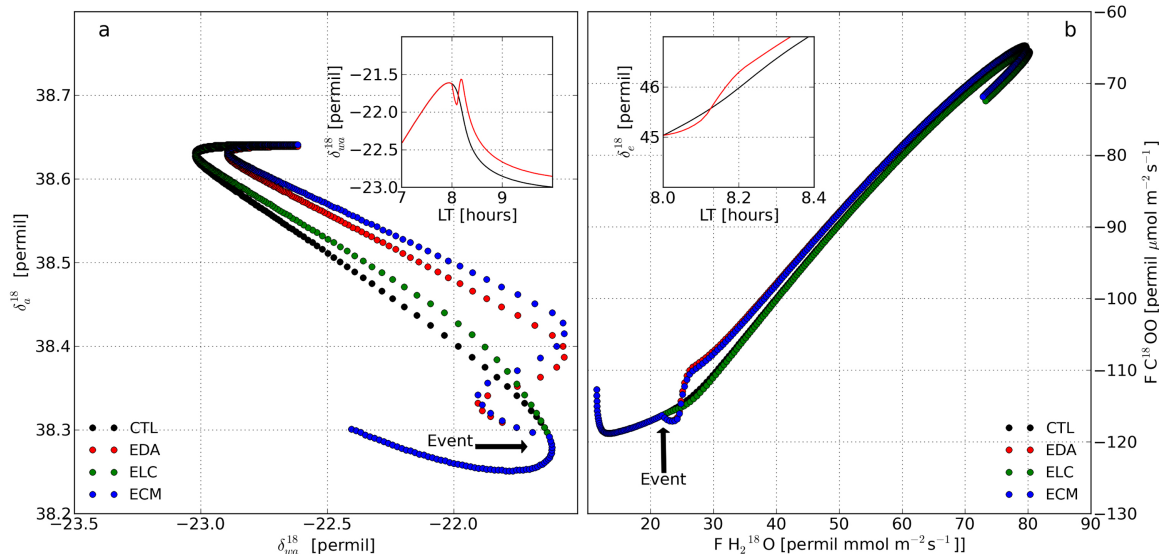


Fig. 11. Diurnal evolution of (a) δ_{wa}^{18} and δ_a^{18} , and (b) the isofluxes for the four experiments. The inset figure shows: in (a) the temporal evolution of δ_{wa}^{18} for the CTL and EDA at the time of the event and (b) the evolution of δ_e^{18} for the CTL and EDA experiments. The arrow marks when the entrainment “Event” begins at 8.01 LT (see temporal evolutions of δ_{wa}^{18} and δ_e^{18} in the inset figures). Each point corresponds to a one-minute sample of δ_a^{18} the model’s results. The results show calculations starting at 7 LT and finishing at 14.5 LT.

heavy isotope $H_2^{18}O$ reaches the surface. The experiment prescribes that for 200 s the dry tongue is characterized by drier air, more specifically $-1.6 \times 10^{-4} \text{ g kg}^{-1}$ less specific humidity (H_2O) and by a lighter isotopic signature, *i.e.* before the event the value in the residual layer is ${}^{FT}\delta_{wa}^{18} = -33.1$ permil and during it ${}^{FT}\delta_{wa}^{18} = -37.6$ permil. Note that the imposed disturbance of q during the event is considerably lower than the ones reported by Couvreux et al. (2006). In the second experiment, the entrained air mass has a lower CO_2 content (ELC), and the air mass entrained is characterised by a higher content of the isotope $C^{18}OO$. More specifically, the isotopic composition of the entrained air is 39.5‰. This is equivalent to a reduction in $^{12}CO_2$ by 0.3 ppm for 200 s. After this period, the CTL values in the residual layer are reimposed. The experiment ECM (entrainment combined) combines the two previous experiments.

Fig. 11a shows a mixing diagram of the evolution of δ_{wa}^{18} versus δ_a^{18} . Each point represents a one-minute *virtual* observation. The observations start at 7 LT and last till 14.5 LT. As indicated by the arrow *Event*, the three experiments have the same values as CTL in the $\delta_{wa}^{18} - \delta_a^{18}$ mixing diagram before the entrainment event is detected by the virtual measurements. Thereafter, the arrival of the entrained air lighter in $H_2^{18}O$ (EDA) and rich in $C^{18}OO$ (ELC) can be observed, leading to non-linear deviations in the isotopic composition for both isotopologues. The inset in Fig. 11a shows deviations of the evolution of δ_{wa}^{18} during the event. In the ECM case, this initially follows the deviation driven by the $H_2^{18}O$ -entrained air. Even after the CTL conditions (for EDA the absolute minimum during the event is δ_{wa}^{18} , equal to $-21.6\text{\textperthousand}$) are restored, the entrainment event disruptions retain information (“memory”) about the change in the isotopic composition during the remaining hours of the experiment.

Fig. 11b presents the results of the three experiments plus the CTL experiments, but now in the isoflux mixing diagram. The deviations after the start of the entrainment event indicate that isofluxes are also influenced by non-local processes, but the changes are less pronounced than in the δ -mixing diagram. This stresses the need to use a modelling framework in which surface and boundary layer processes are coupled. The relationship between the fluxes changes during the entrainment event, due to the variation in the composition of δ_{wa}^{18} and δ_a^{18} and their respective values within the leaf, *i.e.* the δ -gradient. In the EDA experiment, the entrainment of air lighter in $H_2^{18}O$ first leads to more negative values and thereafter to increase in the isoflux of $FC^{18}OO$. As

expressed in our model formulation, the variation on the gradient between the atmospheric value of δ_{wa}^{18} influenced by the entrained lighter residual layer isotopic composition and δ_x (Eq. (A.36)) will lead to variations of the isofluxes.

We discuss the interrelationship between the isofluxes by analysing one aspect of the ECM experiment. Focusing on the isoflux $FC^{18}OO$, its behaviour depends on the gradient $\delta_e^{18} - \delta_a^{18}$ (Eq. (A.24)). The arrival of $C^{18}OO$ -rich air during the entrainment event, which is rich on the isotope composition of $C^{18}OO$ and therefore increases δ_a^{18}), leads to a decrease in the isoflux $FC^{18}OO$ (more negative than the CTL experiment). This decrease is also enhanced due to $FC^{18}OO$ is influenced by changes in δ_{wa}^{18} (in the event drier and lighter air). As shown in the inset Fig. 11b, the dependence on this flux on δ_{wa}^{18} (Eq. (A.26)) leads to a (1) reduction in the δ_e^{18} tendency from 8 to 8.1 LT (more negative values $FC^{18}OO$ than CTL) and (2) a subsequent increase that yields to less negative values $FC^{18}OO$ than CTL. With larger differences (by orders of magnitude), this is a similar effect to that studied by van Heerwaarden et al. (2010), in which a reduction in the atmospheric specific humidity due to dry air entrainment leads to higher rates of evaporation.

The analysis of the four experiments underlines the very high sensitivity of the diurnal evolution of the isotope ratios modelled, not only to the surface fluxes, but also to the composition of the residual layers during the morning transition and, later by the free tropospheric conditions. Three important final remarks: first, high-frequency and precise stable isotopologues measurements are capable of detecting non-local variations in the isotopic composition and their duration. Second, our model framework enables us to disentangle the impact of (non)-local processes on isotope composition. Third, these relationships between δ and isotopologues can be used to improve the interpretation of our observations.

6. Conclusions

Our investigation offers:

- A new modelling framework to study the changes in the stable isotopologues of CO_2 and H_2O under convective atmospheric boundary layer conditions.
- As the atmospheric boundary layer representation is fully coupled to the surface, it enables us to quantify how the individual soil, plant

and entrainment (non-local) processes that contribute to the diurnal variability. The model therefore enables to calculate how the partitioning of these processes influences the sub-hourly variability of the rare and abundant isotopologues of CO₂ and H₂O, ¹³CO₂, C¹⁸OO and H₂¹⁸O.

- The model is specially designed to provide support to field measurements. We evaluate our model by discussing a full comparison with the observations (four-day aggregated case) made above the Harvard Forest. The comparison is systematically presented, and it demonstrates the ability of the model to capture all the essential processes: radiation, surface-energy partitioning, diurnal changes of the potential temperature, specific humidity, CO₂ and H₂O isotopologues, and boundary-layer height.

Our main findings are that:

- With respect to ¹³CO₂, the above-canopy ¹³CO₂ isoflux is characterised by a positive value during the entire day with maximum levels at midday. The model correctly represents the observed morning transition between the nocturnal to the diurnal regime. By calculating the individual contributions using the budget equation, we find that it is during this morning transition that the process of photosynthesis enrich δ_a^{13} . However, we show that this enrichment is partly offset by the entrainment of a residual-layer air mass that is characterised by depleted ¹³CO₂ relative to CO₂, and the less important contribution of soil processes.
- With respect to C¹⁸OO, the observed isoflux above the canopy is characterized by a change of sign, from depletion (negative) of

C¹⁸OO to enrichment (positive) around midday. The Craig-Gordon model is used to model the leaf water isotopic composition under steady-state conditions. Applying a phenomenological formulation, we show that future studies need to take into account the diurnal variability of this composition and the need to have a complete data set to revise all the assumptions including the sub-daily variability of the plant-atmosphere interactions.

- Mixing diagrams of the δ_a^{18} versus δ_w^{18} and the isoflux of C¹⁸OO versus that of H₂¹⁸O show that the entrainment process leads to changes in the relationships that can be detected by measuring of isotope composition.

The model source is available at <http://classmodel.github.io/>. The numerical settings and results of this case study are also available at the same link.

Acknowledgments

We gratefully acknowledge Dr. Rick Wehr (University of Arizona, USA) for providing the stable isotopologue observations.

We thank Harvard Forest for providing the meteorological and carbon dioxide data (<https://harvardforest.fas.harvard.edu/research>). The guidance and comments by two anonymous referee were crucial to improve and sharpen the contents of this research and the model formulation.

Appendix A. Model formulation and definitions

We define the main concepts and equations to implement the isotopologues for water vapor (H₂O) and carbon dioxide (CO₂). Our model is based on mixed-layer model theory and it represents convective boundary layer formed over a coupled surface with active vegetation and soil dynamics. The abundant and light isotopologues are CO₂ and H₂O and the rare and heavy isotopologues are ¹³CO₂, C¹⁸OO and H₂¹⁸O. Here, we follow the stable isotope nomenclature suggested by [Coplen \(2011\)](#).

The governing equations for the state variables and isotopologues in the numerical model are expressed in conserved variables, *i.e.* mixing ratio [ppm or ppb] and flux [ppm m s⁻¹ or ppb m s⁻¹] for the isotopologues, which is in agreement with the other mixed-layer state variables: the potential temperature [K] and specific humidity [kg_w kg_a⁻¹]. Note that in this Appendix, the listed equations are generally valid and written in System International (SI) standard units. Therefore, values of mixing ratios reported in ppb should be multiplied by 10⁻⁹ to be applied in the following equations.

Based on the mixing ratio, we calculate the molar ratio using the mixing ratio calculations of $c_i = \text{CO}_2/\text{CO}_2 + \text{H}_2\text{O}$ (H₂¹⁶O + H₂¹⁸O); the subscript *i* indicates the heavier and less abundant isotopologue.

Our first definition is the isotope ratio that reads:

$$R_i = \frac{c_i}{c} \quad (\text{A.1})$$

Note that throughout the derivation we are not using atomic, *i.e.* isotope, but molecular, *i.e.* isotopologues. The differences between the heavy and light isotopologue are quantified by the δ value

$$\delta_i = \left(\frac{R_i}{R_{\text{ref}}} - 1 \right), \quad (\text{A.2})$$

where R_{ref} is the VSMOW standard for oxygen and VPDB standard for carbon. For the latter, here, following [Wehr et al. \(2013\)](#), we use 0.011057, but we modify the value since $\langle c \rangle$ is the total carbon dioxide: $\text{CO}_2 = \text{CO}_2 + \text{H}_2\text{O}$ (see [Table C.1](#) for the complete information). Note that values for δ , as used in Eq. [\(A.2\)](#) and further on, are usually expressed in per mill *i.e.* values are reported times 10³.

In a similar form as Eq. [\(A.2\)](#), we define a turbulent flux ratio for the isotopologues (F_i) using the δ -notation:

$$\delta_{F_i} = \left(\frac{R_{F_i}}{R_{\text{ref}}} - 1 \right), \quad (\text{A.3})$$

where the turbulent flux ratio R_{F_i} reads

$$R_{F_i} = \frac{\overline{w'c'_i}}{\overline{w'c'}}, \quad (\text{A.4})$$

in which $\overline{w'c'_i}$ and $\overline{w'c'}$ are the turbulent fluxes for the heavy and light isotopologues, respectively.

In the following, we derive the expression that relates $\overline{w'c'_i}$ to the abundant turbulent flux of the isotopologue $\overline{w'c'}$, and the isoflux defined as the product of the concentration of the abundant isotope $\langle c \rangle$ and the flux $\overline{w'\delta}$ ([Lee et al., 2009](#)). The symbol $\langle \cdot \rangle$ means a slab averaged over the entire atmospheric boundary layer following the mixed-layer theory assumptions (Eq. [\(1\)](#)) whereas the symbol \cdot represents a spatial or temporal average.

We derive these relationships using two approaches that lead to the same final expression, as demonstrated below.

A.1 Approach 1

Focusing on a specific fractionation effect, for instance the one occurring during exchange of carbon dioxide between plant and atmosphere, the relationship between the heavy isotopologue surface flux ($\overline{w'c'_i}$) and the light and more abundant isotopologue ($\overline{w'c'}$) are:

$$\overline{w'c'_i} \approx \overline{w'c'} R_i^P. \quad (\text{A.5})$$

We relate these two fluxes by the plant isotopologue ratio R_i^P . In establishing this relation, we assume: (a) R_i^P is representative for R_i at the interface (bidirectionally, from plant to air and from air to plant), and (b) R_i does not fluctuate and is a constant value in our model assumption.

To facilitate the representation, we can further relate R_i^P in Eq. (A.5) to the isotopologue ratio in the atmosphere $\langle R \rangle^a$ by means of an isotopic discrimination α_p . The equation then reads:

$$\overline{w'c'_i} \approx \overline{w'c'} R_i^P \approx \overline{w'c'} \langle R \rangle^a \alpha_p. \quad (\text{A.6})$$

Note that here we introduce $\langle R \rangle^a$ indicating that this variable is calculated using the slab values. Therefore, by taking the slab values from Eq. (A.1), the slab value of $\langle R \rangle^a$ reads:

$$\langle R \rangle^a \approx \frac{\langle c_i \rangle}{\langle c \rangle}. \quad (\text{A.7})$$

In deriving Eq. (A.7) from Eq. (A.1), note that we assume that the fluctuation product $\langle R'c' \rangle$ is much smaller than $\langle c_i \rangle$. Therefore, the term $\langle R'c' \rangle$ is neglected in Eq. (A.7).

Relevant in our formulation is the isotopic fractionating factor α_p . It is related to the isotopic discrimination Δ , in units [%], according to

$$\alpha_p = \frac{R_i^P}{\langle R \rangle^a} \equiv 1 - \Delta. \quad (\text{A.8})$$

Introducing expression (A.8) into Eq. (A.5), the flux $\overline{w'c'_i}$ becomes a function of Δ , and surface and atmospheric properties. It reads

$$\overline{w'c'_i} = \underbrace{\frac{\langle c_i \rangle}{\langle c \rangle} \overline{w'c'}}_I - \underbrace{\frac{\langle c_i \rangle}{\langle c \rangle} \overline{w'c'} \Delta}_\text{III}. \quad (\text{A.9})$$

Note that this expression holds for the flux at all interfaces such as plant-atmosphere, soil-atmosphere or the cloud droplet-environment.

A.2 Approach 2

Here, we closely follow the derivation deduced by L2009 to obtain a relationship that connects the isoflux $\overline{w'\delta'}$ to the isotopologue turbulent flux $\overline{w'c'_i}$.

The derivation starts by calculating the derivative of Eq. (A.2) (Eq. 7 in L2009). We obtain

$$\delta' = \left(\frac{R'}{R_{\text{ref}}} \right) \quad (\text{A.10})$$

Multiplying by the wind vertical velocity fluctuation w' and averaging, we obtain

$$\overline{w'\delta'} = \frac{1}{R_{\text{ref}}} \overline{w'R'}, \quad (\text{A.11})$$

where $\overline{w'\delta'}$ represents the isoflux of the isotopic signature, normally expressed in units % m s⁻¹.

The expression of the molar ratio flux $\overline{w'R'}$ in terms of the surface fluxes $\overline{w'c'_i}$ is derived following Eq. 4 in L2009. The starting point is to derive first the Reynolds fluctuation (R') of the molar ratio R and correlate it to the wind vertical velocity fluctuation w' . First, we calculate R' :

$$\begin{aligned} R' &= \left(\frac{c_i}{c} \right)' \\ &= \left(c_i \frac{1}{c} \right)' \\ &= c'_i \frac{1}{c} + c_i \left(\frac{1}{c} \right)' \\ &= c'_i \frac{1}{c} + c_i \left(-\frac{c'}{c^2} \right) \\ &= \frac{1}{c} \left(c'_i - \frac{c_i}{c} c' \right) \\ &= \frac{1}{c} (c'_i - R c') \\ &\approx \frac{1}{\langle c \rangle} (c'_i - \langle R \rangle c'). \end{aligned} \quad (\text{A.12})$$

In the final approximation, we substitute $c = \langle c \rangle + c'$ and $R = \langle R \rangle + R'$ and subsequently we assume that $\langle c \rangle > c'$ and $\langle R \rangle > R'$. By correlating R' to the vertical velocity fluctuation w' and averaging, we obtain:

$$\overline{w'R'} = \frac{\overline{w'c'}}{\langle c \rangle} \left(\frac{\overline{w'c'_i}}{\overline{w'c'}} - \langle R \rangle \right). \quad (\text{A.13})$$

Introducing this turbulent flux $\overline{w'R'}$ into Eq. (A.11), the expression of $\overline{w'\delta'}$ becomes:

$$\overline{w'\delta'} = \frac{1}{R_{\text{ref}}} \left[\frac{\overline{w'c'_i}}{\overline{w'c'}} - \langle R \rangle \right] \frac{\overline{w'c'}}{\langle c \rangle}. \quad (\text{A.14})$$

Reordering this expression and using $\langle R \rangle = \langle c_i \rangle / \langle c \rangle$, the final expression for $\overline{w'c'_i}$ to be implemented in the soil-plant-atmospheric model becomes:

$$\underbrace{\overline{w'c'_i}}_I = \underbrace{\frac{\langle c_i \rangle}{\langle c \rangle} \overline{w'c'}}_{\text{II}} + \underbrace{\frac{R_{\text{ref}} \langle c \rangle \overline{w'\delta'}}{\overline{w'c'}}}_{\text{III}}. \quad (\text{A.15})$$

As defined by Eq. (6), the product $\langle c \rangle \overline{w'\delta'}$, the isoflux, is the quantity to be compared against the measurements.

A.3 Equivalence between approaches 1 and 2

In the following we show that Eq. (A.9) is equivalent to Eq. (A.15). The heavy isotopologue flux, terms I, are equal. The scaled isotopologue flux for the light compound, terms II in both equations, are also equal. Below we demonstrate the equivalence of terms III. We start with term III in Eq. (A.15). Using Eqs. (A.11) and (A.13), we obtain

$$\begin{aligned} R_{\text{ref}} \langle c \rangle \overline{w'\delta'} &= \langle c \rangle \overline{w'R'} \\ &= \overline{w'c'} \left(\frac{\overline{w'c'_i}}{\overline{w'c'}} - \langle R \rangle^a \right) \\ &= \overline{w'c'} \langle R \rangle^a \left(\frac{\overline{w'c'_i}}{\overline{w'c'}} - \frac{1}{\langle R \rangle^a} - 1 \right). \end{aligned}$$

In the last step, we have factorized by $\langle R \rangle^a$. By rewriting the first term in the bracket by Eq. (A.6), and thereafter using Eq. (A.8), the final expression reads:

$$R_{\text{ref}} \langle c \rangle \overline{w'\delta'} = \overline{w'c'} \langle R \rangle^a (\alpha_p - 1) = -\langle R \rangle^a \overline{w'c'} \Delta. \quad (\text{A.16})$$

This last term in Eq. (A.16) is equal to the second term on the r.h.s of Eq. (A.15).

This last derived relation enable us to relate the isoflux $\overline{w'\delta'}$ to the turbulent flux of the more abundant isotopologue and the gradient between surface (either soil or plant) and atmospheric δ -values as follows:

$$\begin{aligned} (\overline{w'\delta'}) &= \frac{\overline{w'c'} \langle R \rangle^a}{\langle c \rangle R_{\text{ref}}} (-\Delta) \\ &= \frac{\overline{w'c'} \langle R \rangle^a}{\langle c \rangle R_{\text{ref}}} (\alpha - 1) \\ &= \frac{\overline{w'c'} \langle R \rangle^a}{\langle c \rangle} \left(\frac{\overline{w'c'_i}}{\overline{w'c'}} \frac{1}{R} - 1 \right) \frac{1}{R_{\text{ref}}} \\ &= \frac{\overline{w'c'}}{\langle c \rangle} (\delta_{\text{Fi}} - \delta), \end{aligned} \quad (\text{A.17})$$

where δ_{Fi} (i representing either plant or soil) and δ represents the isotopic signature of the turbulent flux and the atmospheric mixing ratio, respectively.

A.4 Plant and soil flux representations in the mixed-layer model

We employ Eq. (A.15) to represent the surface turbulent fluxes for $^{13}\text{CO}_2$, C^{18}OO and H_2^{18}O . In the following sections, we present the specific expressions of plant ($\overline{w'\delta'}_{\text{plant}}$) and soil ($\overline{w'\delta'}_{\text{soil}}$) for the isotopologues $^{13}\text{CO}_2$, C^{18}OO and H_2^{18}O to be introduced in Eq. (A.15).

A.4.1 Flux of $^{13}\text{CO}_2$

The specific expressions for the flux of $^{13}\text{CO}_2$ (Eq. (A.15)) for plant and soil as a function of $\overline{w'\delta'}$ are given below.

1 Plant:

For the flux related to plant assimilation we apply Eq. (24) from L2009:

$$\overline{w'\delta'}_{\text{plant}} = - \frac{\overline{w'c'}_{\text{plant}}}{\langle c \rangle} \Delta, \quad (\text{A.18})$$

where Δ for $^{13}\text{CO}_2$ reads:

$$\Delta = \left[\epsilon_k^{13} + (b - \epsilon_k^{13}) \frac{c_{\text{leaf}}}{\langle c \rangle} \right], \quad (\text{A.19})$$

Δ is the isotopic discrimination representing the diffusion processes during photosynthesis.

The other variables and parameters are:

- $\frac{r_c}{\langle c \rangle}$: ratio of the plant internal stomatal concentration at the leaf scale to the atmospheric concentration. It is calculated by the A-gs model (Ronda et al., 2001; Vilà-Guerau de Arellano et al., 2015) as a function of water vapor deficit.
- $\overline{w'c'}$ _plant: CO₂ plant assimilation turbulent flux at the canopy scale. In calculating this term using the A-gs model, we first calculate it at leaf level and is subsequently upscaled it to the canopy level.
- ϵ_k^{13} : fractionation by diffusion. It reads:

$$\epsilon_k^{13} = \frac{2.9r_b^c + 4.4r_c^c}{r_a + r_b^c + r_c^c}, \quad (\text{A.20})$$

in which r_a , r_b^c and r_c^c are the aerodynamic, boundary and surface canopy resistances, respectively.

- b: fractionation by carboxylation 27.0‰

2 Soil:

The soil isoflux reads:

$$\overline{w'\delta'}_{\text{soil}} = \frac{\overline{w'c'}_{\text{soil}}}{\langle c \rangle} [\delta_R^{13} - \delta_a], \quad (\text{A.21})$$

where

- δ_R^{13} : -28.0‰. This value of soil respiration (R) depends on the ecosystem characteristics and the age of the soil. In absence of data at Harvard Forest, here we prescribe a similar value as in L2009.
- $\overline{w'c'}_{\text{soil}}$: CO₂ efflux soil respiration calculated as a function of the soil temperature and soil moisture stress (Jacobs et al., 2007). The expression for $\overline{w'c'}_{\text{soil}}$ reads:

$$\overline{w'c'}_{\text{soil}} = R_{10} (1 - f(w)) e^{\left[\left(\frac{E_0}{283.15 R^*} \right) \left(1 - \frac{283.15}{T_{\text{soil}} + 273.15} \right) \right]}, \quad (\text{A.22})$$

where R^* is the universal gas constant (units $\text{kJ kmol}^{-1} \text{K}^{-1}$), E_0 is the activation energy, T_{soil} is the temperature of the soil layer interacting with the atmosphere, R_{10} is the respiration rate at 10 °C under conditions of no water-stress soil. Compared to Vilà-Guerau de Arellano et al. (2015), the value employed in our numerical settings at the Harvard Forest is $R_{10} = 0.18 \text{ mg CO}_2 \text{ m}^{-2} \text{ s}^{-1}$ (equivalent to $4.1 \mu\text{mol m}^{-2} \text{ s}^{-1}$). Finally $f(w)$ is a function to adjust the CO₂ soil respiration under conditions of soil water stress. It reads:

$$f(w) = C \frac{w_{\max}}{w + w_{\min}}. \quad (\text{A.23})$$

w is the soil moisture content (depending on the root depth at soil level 1 or 2), w_{\max} and w_{\min} are respectively 0.55 and 0.005 representing reference values of the soil water content. The constant C is taken equal to 1.6×10^{-3} .

A.4.2 Flux of C¹⁸OO

Similar to the flux of ¹³CO₂, here we follow closely the formulation suggested by L2009, and references therein, unless it is indicated otherwise.

1 Plant

$$\overline{w'\delta'}_{\text{plant}} = \frac{\overline{w'c'}_{\text{plant}}}{\langle c \rangle} \left[\frac{c_{\text{cs}}}{c_{\text{cs}} - \langle c \rangle} (\delta_e^{18} - \delta_a^{18}) \theta_{\text{eq}} + (1 - \theta_{\text{eq}}) \epsilon_k^{18} \frac{c_{\text{cs}}}{\langle c \rangle} - \epsilon_k^{18} \right], \quad (\text{A.24})$$

where θ_{eq} is the degree of oxygen isotope equilibration between CO₂ and H₂O at leaf level, i.e. it is the degree of hydration in leaves. In our model, it is a constant value (see below). δ_a^{18} can be calculated from Eqs. (A.1) and (A.2) and the ratio $\frac{c_{\text{cs}}}{\langle c \rangle}$ is explicitly calculated in the A-gs model (see calculation below).

The key element of the parameterization is how to represent the value of ¹⁸O in equilibrium with leaf water δ_e^{18} . The expression reads:

$$\delta_e^{18} = \left(\delta_L^w + \frac{17604}{(T_c + 273.16)} - 17.93 \right). \quad (\text{A.25})$$

T_c is the canopy temperature (in Celsius) and δ_L^w is the ¹⁸O isotopic composition of evaporative water in the leaf.

The expression (A.25) represents the contribution of two processes that describe oxygen isotope exchange between CO₂ and H₂O at the leaf surface within the atmospheric temperature range. It first considers the process related to the equilibrium of the ¹⁸O between water vapor and carbon dioxide within the water. Here, we follow the expression proposed by Brenninkmeijer et al. (1983) that depends on the temperature T_c . In our modelling framework we relate to the canopy temperature to the surface temperature (right-hand-side term in Eq. (A.25)).

Secondly, the representation includes plant transpiration under steady-state conditions (term δ_L^w in Eq. (A.25)). We use the expression proposed by Gillon and Yakir (2001) inspired on the seminal study of Craig–Gordon (Craig and Gordon, 1965). The expression for δ_e^{18} (equilibrium state) reads:

$$\delta_L^w = \delta_{ss} = \delta_x + \epsilon_{eq} + \epsilon_k^w + RH (\delta_{wa}^{18} - \epsilon_k^w - \delta_x) \alpha_{eq}, \quad (A.26)$$

where $\delta_x = -5\%$ is the isotopic signature driven by the xylem and we use a value estimated for $H_2^{18}O$. RH is the relative humidity at the leaf surface and δ_a^{18} is calculated according to Eqs. (A.1) and (A.2). Note that the stable isotopic fractionation factor α_{eq} (defined in Eq. (A.29)) represents the preference of ^{18}O to reside in liquid or water vapor. It is related to the equilibrium fractionation ϵ_{eq} (defined at Eq. (A.28)). This ^{18}O isotopic composition of leaf water evaporation is normally assumed to be in an equilibrium state (Zhang et al., 2009).

In Eq. (A.26), ϵ_k^w represents the weighted mean kinetic fractionation accounting for the laminar leaf boundary layer resistance (r_b), turbulent aerodynamic resistance (r_a) and the stagnant substomatal cavity resistance (r_c) (see Vilà-Guerau de Arellano et al. (2015) for more information). It reads:

$$\epsilon_k^w = \frac{21r_b^w + 32r_c^w}{r_a + r_b^w + r_c^w}. \quad (A.27)$$

Notice that r_c^w and r_a are larger than r_c^c , and therefore we omit this resistance in Eq. (A.27). If needed, we can use expressions as a function of mean wind speed (see Eq. (A3), as suggested by L2009). r_a is the aerodynamic resistance and r_c^c is the canopy resistance.

In Eq. (A.26), the equilibrium fractionation ϵ_{eq} depends on the equilibrium fractionation factor α_{eq} . This factor α is defined as $\frac{R_p}{R_r}$ where the subscripts p and r are generic ratios in different phases of a substance. Here, following L2009, we employ:

$$\epsilon_{eq} = \left(1 - \frac{1}{\alpha_{eq}}\right). \quad (A.28)$$

where α_{eq} is expressed as:

$$\alpha_{eq} = e^{\left(\frac{1137}{(T_c + 273.16)^2} - \frac{0.4156}{(T_c + 273.16)} - 2.0667 \cdot 10^{-3}\right)} \quad (A.29)$$

A typical value of $\epsilon_{eq} = 9.8\%$ at $T = 20^\circ C$. In agreement with the values obtained by L2009 for forest, the kinetic fractionation ϵ_k^w (Eq. (A.27)) for $H_2^{18}O$ is 27% with small diurnal variation.

To complete the explanation for the representation of Eq. (A.24), we need to introduce the canopy-scale kinetic fractionation factor due to diffusion. ϵ_k^{18} depends on the aerodynamic and canopy resistance (Eq. (A.30)). The canopy-scale fractionation factor for $C^{18}OO$ reads:

$$\epsilon_k^{18} = \frac{5.8r_b^c + 8.8r_c^c}{r_a + r_b^c + r_c^c}, \quad (A.30)$$

For our Harvard Forest case the value is almost constant on time and equal to 7.9%.

Lastly, $\overline{w'\delta'}$ plant in Eq. (A.24) depends on the degree of oxygen equilibration between CO_2 and leaf water (θ_{eq}). We are aware that $\overline{w'\delta'}$ plant calculations are sensitive to this value (Gangi et al., 2015). Based on sensitivity analysis we selected the value 0.75 based on the best fit with observations. Note that in the ideal case that CO_2 in the intercellular space is in full isotopic equilibrium with the leaf water, then $\theta_{eq} = 1$. For our case, and based on sensitivity analysis, we prescribe the value 0.75. Note that in that case Eq. (A.24) is simplified to (Eq. (13) in L2009):

$$\overline{w'\delta'}$$
 plant = $\frac{\overline{w'c'}}$ plant $\left[\frac{c_{cs}}{c_{cs} - \langle c \rangle} (\delta_e^{18} - \delta_a^{18}) - \epsilon_k^{18} \right], \quad (A.31)$

The last variable and their dependencies on meteorology and leaf processes in Eq. (A.24) is the mixing ratio in the chloroplast (c_{cs}) is calculated using:

$$c_{cs} = c_{leaf} - \frac{A}{g_m}, \quad (A.32)$$

where A is the leaf net assimilation, c_{leaf} is the mixing ratio in the intercellular air inside the leaf and g_m is the mesophyll conductance. In our numerical set up, these variables are calculated by the A-gs model. Note that in the A-gs model the fraction between the leaf and atmosphere mixing ratio is a function of the vapour pressure deficit (Ronda et al., 2001; Vilà-Guerau de Arellano et al., 2015).

Two final notes in the formulation of $\overline{w'\delta'}$ plant. Note that the upscaling to the canopy level is included in the turbulent flux $\overline{w'c'}$ plant in Eq. (A.24). Note that in our calculations of $C^{18}OO$ we employ the R_{ref} standard of $C^{18}OO$ (VSMOW) equal to 0.0020052 for $^{18}O/^{16}O$ (Baertschi, 1976). For this molecule, this standard value is multiplied by a factor 2 to take into account that the ^{18}O can be substituted at both oxygen atom positions of CO_2 .

2 Soil:

Following Eq. (13) in L2009, we use the following expression for the isoflux to represent the soil-atmosphere exchange:

$$\overline{w'\delta'}$$
 soil = $\frac{\overline{w'c'}}$ soil $\left[\frac{c_{soil}}{c_{soil} - \langle c \rangle} (\delta_s^{18} - \delta_a^{18}) - \epsilon_{k,s}^{18} \right]. \quad (A.33)$

- δ_s^{18} : isotopic composition of soil CO_2 assumed to be in full equilibrium with soil water whose isotopic composition is interpolated between weekly measurements at a depth of 10 cm. Following L2009, we prescribe a constant value equal to -28% .

- $\epsilon_{k,s}^{18}$: kinetic fractionation for soil respiration is

$$\epsilon_{k,s}^{18} = \frac{8.8r_s^c}{r_a + r_{a,s} + r_s^c}, \quad (\text{A.34})$$

where r_a is the aerodynamic resistance (calculated explicitly in the soil-plant-atmosphere model). L2009 suggested for the soil resistance r_s^c a value of 800 s m^{-1} (Appendix A). We assume the aerodynamic resistance between the soil surface and canopy top ($r_{a,s}$) is smaller than the other two other resistance, r_a and r_s^c , under convective boundary layer conditions.

- c_{soil} : molar concentration of CO_2 in the soil pore space is calculated according to

$$c_{\text{soil}} = \langle c \rangle + \overline{w'c'}_{\text{soil}} (r_a + r_{a,s} + r_s^c), \quad (\text{A.35})$$

Here we use the same expression for $\overline{w'c'}_{\text{soil}}$ as expressed at Eq. (A.22). We also increase the soil resistance r_s^c by 25% to obtain realistic values of the soil mixing ratio for carbon dioxide in forests (see Fig. 6).

A.4.3 Flux of $H_2^{18}\text{O}$

1 Plant:

Here we take the formulation proposed by Lee et al. (2012), assuming that the canopy transpiration is in isotopic steady state:

$$\overline{w'\delta'}_{\text{plant}}^w = \frac{\overline{w'q'}_{\text{plant}}}{\langle q_a \rangle} (\delta_x - \delta_{\text{wa}}^{18}) \quad (\text{A.36})$$

where $\overline{w'q'}_{\text{plant}}$ is the evapotranspiration at canopy scale by plants (calculated using A-gs and the surface energy balance), δ_x is the ^{18}O composition of the xylem water with the same value as the soil water ($-5\text{\textperthousand}$). It needs to be stressed that δ_{wa}^{18} refers to the ^{18}O in the water vapour isotopologue.

2 Soil:

Lee et al. (2012) assumed a fully-leaf ecosystem (soil evaporation is much smaller than transpiration). In our modelling framework, we can represent the differences between soil evaporation and plan transpiration using the vegetation cover parameter: c_{veg} and a specific representation for the soil evaporation applied to the fraction ($1 - c_{\text{veg}}$). The expression therefore reads:

$$\overline{w'\delta'}_{\text{soil}} = \frac{\overline{w'q'}_{\text{soil}}}{q_a} (\delta_x - \delta_{\text{wa}}^{18}) \quad (\text{A.37})$$

where $\overline{w'q'}_{\text{soil}}$ is the soil evaporation (calculated using a two-layer force soil restored model (Vilà-Guerau de Arellano et al., 2015)), δ_x is the ^{18}O composition of xylem water with the same value as the soil water ($-5\text{\textperthousand}$), and δ_{wa}^{18} is the isotopic composition of atmospheric water vapour.

A.5 Derivation of the δ -budget

Below we present the derivation of the budget equation as used to calculate the surface and entrainment contributions (see final Eq. (7) in main text).

$$\frac{\partial \delta}{\partial t} = \frac{1}{R_{\text{ref}}} \frac{\partial R}{\partial t} = \frac{1}{R_{\text{ref}}} \frac{\partial}{\partial t} \left(\frac{\langle c_i \rangle}{\langle c \rangle} \right) = \quad (\text{A.38})$$

$$\begin{aligned} & \frac{1}{R_{\text{ref}}} \frac{1}{\langle c \rangle^2} \left(\langle c \rangle \frac{\partial \langle c_i \rangle}{\partial t} - \langle c_i \rangle \frac{\partial \langle c \rangle}{\partial t} \right) = \\ & \frac{1}{R_{\text{ref}}} \frac{1}{\langle c \rangle} \frac{1}{h} \left([\langle w'c'_i \rangle_s - \langle w'c'_i \rangle_e] - \frac{\langle c_i \rangle}{\langle c \rangle} [\langle w'c' \rangle_s - \langle w'c' \rangle_e] \right). \end{aligned}$$

In the last step of the derivation, we use Eq. (1) and substitute $\frac{\partial \langle c_i \rangle}{\partial t}$ and $\frac{\partial \langle c \rangle}{\partial t}$ by the respective mixed-layer equation. Note that the advective term is neglected.

In order to obtain the final expression Eq. (7), we substitute the surface flux of the heavy isotope $(\overline{w'c'_i})_s$ by expression Eq. (3). After rearranging the expression reads:

$$\frac{\partial \delta}{\partial t} = \frac{1}{R_{\text{ref}}} \frac{1}{\langle c \rangle} \frac{1}{h} [R_{\text{ref}} \langle c \rangle \overline{w'\delta'} - (\overline{w'c'_i})_e + \frac{\langle c_i \rangle}{\langle c \rangle} (\overline{w'c'})_e]. \quad (\text{A.39})$$

The last step in the derivation is to substitute the entrainment fluxes by the generic parameterization expressed by Eq. (5). Note that the subsidence vertical velocity is omitted. The new expression is:

$$\frac{\partial \delta}{\partial t} = \frac{1}{R_{\text{ref}}} \frac{1}{\langle c \rangle} \frac{1}{h} \left[R_{\text{ref}} \langle c \rangle \overline{w'\delta'} + \frac{\text{entrainment}}{\frac{\partial h}{\partial t} (c_i^{\text{FT}} - \langle c_i \rangle) - R^a (c^{\text{FT}} - \langle c \rangle)} \right], \quad (\text{A.40})$$

where R^a is $\frac{\langle q \rangle}{\langle c \rangle}$. We now only manipulate and rearrange the entrainment term

$$\frac{\partial h}{\partial t}((c_i^{\text{FT}} - \langle c_i \rangle) - R^a (c^{\text{FT}} - \langle c \rangle)) = \frac{\partial h}{\partial t} \left(\left(\frac{c_i^{\text{FT}}}{c^{\text{FT}}} c^{\text{FT}} - \frac{\langle c_i \rangle}{\langle c \rangle} \langle c \rangle \right) - R^a \left(c^{\text{FT}} - \langle c \rangle \right) \right). \quad (\text{A.41})$$

Introducing now $R^a = \frac{\langle c \rangle}{\langle c_i \rangle}$ and $R^{\text{FT}} = \frac{c_i^{\text{FT}}}{c^{\text{FT}}}$, the second and fourth term cancel. The expression reads:

$$\frac{\partial h}{\partial t}((c_i^{\text{FT}} - \langle c_i \rangle) - R^a (c^{\text{FT}} - \langle c \rangle)) = \frac{\partial h}{\partial t} (R^{\text{FT}} c^{\text{FT}} - R^a c^{\text{FT}}), \quad (\text{A.42})$$

$$\frac{\partial h}{\partial t} (R^{\text{FT}} c^{\text{FT}} - R^a c^{\text{FT}}), \quad (\text{A.43})$$

and dividing and multiplying by the heavy-to-light isotope standard value R_{ref}

$$\frac{\partial h}{\partial t}((c_i^{\text{FT}} - \langle c_i \rangle) - R^a (c^{\text{FT}} - \langle c \rangle)) = \frac{\partial h}{\partial t} c^{\text{FT}} R_{\text{ref}} \left(\frac{R^{\text{FT}}}{R_{\text{ref}}} - \frac{R^a}{R_{\text{ref}}} \right) = \quad (\text{A.44})$$

$$\frac{\partial h}{\partial t} c^{\text{FT}} R_{\text{ref}} (\delta^{\text{FT}} - \delta^a). \quad (\text{A.45})$$

Substituting now the rearranged entrainment term at Eq. (A.40), the final expression used to calculate the δ –budget (Eq. (7)) reads:

$$\begin{aligned} \frac{\partial \delta}{\partial t} &= \frac{1}{R_{\text{ref}}} \frac{1}{\langle c \rangle} \frac{1}{h} [R_{\text{ref}} \langle c \rangle \overline{w' \delta'} + \frac{\partial h}{\partial t} c^{\text{FT}} R_{\text{ref}} (\delta^{\text{FT}} - \delta^a)] \\ &= \frac{1}{h} \left[\overline{w' \delta'} + \left(\frac{\partial h}{\partial t} \right) \left(\frac{c^{\text{FT}}}{\langle c \rangle} \right) (\delta^{\text{FT}} - \delta^a) \right]. \end{aligned} \quad (\text{A.46})$$

Appendix B. New formulation isoflux C¹⁸OO

We propose an expression for the flux $\overline{w' \delta'_{\text{plant}}}$ based on the leaf water isotopic composition measurements (Cernusak et al., 2002). We formulate PAR2 as an attempt to introduce explicitly the temporal evolution of the isotopic composition leaf water. It is a phenomenological representation based on observations (Cernusak et al., 2002), and it still requires a more thorough observational validation. Potential improvements on the Craig–Gordon representation need to take into account the diurnal variability of the leaf water isotopic composition. The expression reads:

$$\overline{w' \delta'_{\text{plant}}} = \frac{\overline{w' c'_{\text{plant}}}}{\langle c \rangle} (\delta_{\text{eff}}^{18\text{O}} - \delta_a^{18}). \quad (\text{B.1})$$

Here $\delta_{\text{eff}}^{18\text{O}}$ represents an effective signature of C¹⁸OO based on measurements of the diurnal variability of $\delta_L^{18\text{O}}$. We call it effective since it includes the effects of diffusion and water equilibrium in discriminating C¹⁸OO from CO₂. Similar to PAR1, $\overline{w' \delta'_{\text{plant}}}$ is proportional to the turbulent flux of the abundant isotopologue scaled by the mixed-layer value $\langle c \rangle$ and the gradient between the laminar leaf water $\delta_{\text{eff}}^{18\text{O}}$ and the atmospheric value δ_a^{18} . The proposed expression for $\delta_{\text{eff}}^{18\text{O}}$ reads:

$$\delta_{\text{eff}}^{18\text{O}} = A \sin \left(\frac{t - t_{\text{daystart}}}{t_{\text{diurnal}}} - \frac{\pi}{B} \right) + C, \quad (\text{B.2})$$

in which t_{daystart} and t_{diurnal} are the starting time of the model experiment and the period of the diurnal cycle, respectively. The constants A , B and C are 25‰, 8 and 15‰. These constants are obtained by fitting a function to the diurnal variation observed in the oxygen isotope ratio of $\delta_L^{18\text{O}}$ measured by Cernusak et al. (2002) and Gangi et al. (2015) in leaf water and they can require adjustment depending on the plant and availability of observations. Here, we assume that inside the mesophyll the ¹⁸O of CO₂ depends on H₂O. As a result, we assume that they equilibrate and therefore are almost independent on time. A similar independent behaviour with time is assumed for the fractionation during diffusion. Therefore, the leaf water composition is the only process substantially varying with time. Note that our representation includes an offset represented by the constant C to account for the fractionation between CO₂ and H₂O in equilibrium (Brenninkmeijer et al., 1983).

Appendix C. Numerical experiments settings

Table C.1 includes the initial vertical profiles for the thermodynamic state variables and the isotopologues. If observations are available, the initial conditions are set accordingly. For the stable isotopologues, the δ –values are converted to mixing ratio using the CO₂ mixing ratio and the H₂O specific humidity. It is important to note that we need to adapt these conditions slightly to account for the assumption of an infinitesimally thin inversion layer (see Fig. 1).

Table C.2

Table C.1

Initial and boundary conditions of the atmospheric state and isotopologue variables employed to represent the four-successive days as an aggregate day: 16–19 September 2011 over the Harvard Forest. The initial conditions are prescribed at 12 UTC (07 local time).

Initial boundary layer height	100 m
Large scale subsidence velocity (w_s)	0 ms^{-1}
<i>Potential temperature</i>	
0 m < z < 100 m	283.3 K
z > 100 m	285.3 + 3.0 10^{-3} ($z - 100$) K
<i>Specific humidity</i>	
0 m < z < 100 m	5.7 $\text{g}_w \text{kg}_d^{-1}$
z > 100 m	5.6–1.8 10^{-3} ($z - 100$) $\text{g}_w \text{kg}_d^{-1}$
<i>Carbon dioxide</i>	
0 m < z < 100 m	389.0 ppm
z > 100 m	380.5 ppm
$^{13}\text{CO}_2$ using $R_{\text{VPDB}}^{13} = 0.011057$ ⁽¹⁾	
0 m < z < 100 m	4.266 ppm ($\delta = -8.17\text{\textperthousand}$)
z > 100 m	4.174 ppm ($\delta = -7.88\text{\textperthousand}$)
^{18}OO using $R_{\text{VSMOW}}^{18} \approx 0.0040104$ ⁽²⁾	
0 m < z < 100 m	1.6198 ppm ($\delta = 37.79\text{\textperthousand}$)
z > 100 m	1.5850 ppm ($\delta = 38.69\text{\textperthousand}$)
H_2^{18}O using $R_{\text{VSMOW}}^{18} = 0.0020052$	
0 m < z < 100 m	ppm ($\delta = -22.08\text{\textperthousand}$)
z > 100 m	17.6440 – 5.7($z - 100$) ppm ($\delta = -22.27\text{\textperthousand}$)

(1) This value is for $\text{CO}_2 = ^{12}\text{CO}_2 + ^{13}\text{CO}_2$.
The value for $^{12}\text{CO}_2$ as basis is
 $R_{\text{VPDB}}^{13} = 0.0111797$.

(2) Oxygen is contained twice in the isotopologue.
Therefore the value is multiplied by the factor 2

Table C.2

Initial and boundary conditions for the vegetation and soil models employed to represent the four-successive days as an aggregate day: 16–19th September 2011 over the Harvard Forest. The initial conditions are prescribed at 12 UTC (07 local time).

Variable	Description and unit	Harvard forest
Geographic and time:		
Lat	Latitude [deg]	42.5 N
Lon	Longitude [deg]	72.2 W
DOY	Day of the year [-]	262.
Time	Initial time [UTC]	12.
Vegetation:		
LAI	Leaf area index of vegetated surface fraction [-]	3.5
C_{veg}	Vegetation cover [-]	0.75
$r_{c,min}$	Minimum resistance transpiration [s m^{-1}]	500.
$r_{s,soil,min}$	Minimum resistance soil evaporation [s m^{-1}]	50.
g_D	VPD correction factor for surface resistance [-]	0.3
z_{0m}	Roughness length for momentum [m]	2.
z_{0h}	Roughness length for heat and moisture [m]	2.
α	surface albedo [-]	0.15
W_l	Equivalent water layer depth for wet vegetation [m]	0
Soil:		
T_s	Initial surface temperature [K]	284.
T_{soil1}	Temperature top soil layer [K]	278.
T_{soil2}	Temperature deeper soil layer [K]	274.
w_{sat}	Saturated volumetric water content [$\text{m}^3 \text{m}^{-3}$]	0.472
w_{fc}	Volumetric water content field capacity [$\text{m}^3 \text{m}^{-3}$]	0.323
w_{wilt}	Volumetric water content wilting point [$\text{m}^3 \text{m}^{-3}$]	0.171
w_{soil1}	Volumetric water content top soil layer [$\text{m}^3 \text{m}^{-3}$]	0.235
w_{soil2}	Volumetric water content deeper soil layer [$\text{m}^3 \text{m}^{-3}$]	0.235
a	Clapp and Hornberger retention curve parameter [-]	0.219
b	Clapp and Hornberger retention curve parameter [-]	4.9
p	Clapp and Hornberger retention curve parameter [-]	4.0
CG_{sat}	saturated soil conductivity for heat [$\text{K m}^{-2} \text{J}^{-1}$]	3.56×10^{-6}
$C1_{\text{sat}}$	Coefficient force term moisture [-]	0.342
$C2_{\text{ref}}$	Coefficient restore term moisture [-]	0.3
Λ	Thermal diffusivity skin layer [-]	30

References

- Baertschi, P., 1976. Absolute ^{18}O content of standard mean ocean water. *Earth Planet. Sci. Lett.* 31, 341–344.
- Baldocchi, D., Bowling, D.R., 2003. Modelling the discrimination of $^{13}\text{CO}_2$ above and within a temperate broad-leaved canopy on hourly to seasonal time scales. *Plant Cell Environ.* 26, 231–244.
- Bauer, P., Thorpe, A., Brunet, G., 2015. The quite revolution of numerical weather prediction. *Nature* 525, 47–55.
- Bekele, A., Kellman, L., Beltrami, H., 2007. Soil profile CO_2 concentrations in forest and clear cut sites in Nova Scotia, Canada. *For. Ecol. Manag.* 242, 587–597.
- Bickford, C.P., McDowell, N.G., Erhardt, E.B., Hanson, D.T., 2009. High-frequency field measurements of diurnal carbon isotope discrimination and internal conductance in a semi-arid species *Juniperus monosperma*. *Plant Cell Environ.* 32, 796–810.
- Bowling, D., Tans, P., Monson, R., 2001. Partitioning net ecosystem exchange carbon exchange with isotopic fluxes of CO_2 . *Glob. Change Biol.* 7, 127–145.
- Brenninkmeijer, C.A.M., Kraft, P., Mook, W.G., 1983. Oxygen isotope fractionation between CO_2 and H_2O . *Isotope Geosci.* 1, 181–190.
- Cernusak, L.A., Pate, J.S., Farquhar, G.D., 2002. Diurnal variation in the stable isotope composition of water and dry matter in fruiting *Lupinus angustifolius* under field conditions. *Plant Cell Environ.* 25, 893–907.
- Conzemius, R., Fedorovich, E., 2006. Dynamics of sheared convective boundary layer entrainment. Part II: Evaluation of bulk model predictions of entrainment flux. *J. Atmos. Sci.* 63, 1179–1199.
- Coplen, T.B., 2011. Guidelines and recommended terms for expression of stable-isotope-ratio and gas-ratio measurements results. *Rapid Commun. Mass Spectrom.* 25, 2538–2560.
- Couvreux, F., Guichard, F., Redelsperger, J., Kiemle, C., Masson, V., Lafore, J., Flamant, C., 2006. Water-vapour variability within a convective boundary-layer assessed by large-eddy simulations and the IHOP-2002 observations. *Q. J. R. Meteorol. Soc.* 131, 2665–2693.
- Craig, H., Gordon, L.I., 1965. Deuterium and oxygen-18 variations in the ocean and the marine atmosphere. In: Tongiorgi, E. (Ed.), *Proceedings of a Conference on Stable Isotopes in Oceanographic Studies and Paleotemperatures*, pp. 9–130.
- Flexas, J., Ribas-Carbo, M., Diaz-Espejo, A., Gallego, J., Medrano, H., 2008. Mesophyll conductance to CO_2 : current knowledge and future prospects. *Plant Cell Environ.* 31, 602–621.
- Foken, T., 2008. The energy balance closure problem: an overview. *Ecol. Appl.* 18, 1351–1367.
- Gangi, L., Tabbe, W., Vereecken, H., Brügelmann, N., 2015. Effect of short term variations of environmental conditions on atmospheric CO^{18}O iso forcing of different plant species. *Agric. For. Meteorol.* 201, 128–141.
- Gillon, J., Yakir, D., 2001. Influence of carbonic anhydrase activity in terrestrial vegetation on the ^{18}O content of atmospheric CO_2 . *Science* 291, 2584–2587.
- Griffis, T.J., 2013. Tracing the flow of carbon dioxide and water vapor between the biosphere and atmosphere: a review of optical isotope techniques and their application. *Agric. For. Meteorol.* 174–175, 85–109.
- Jacobs, A.F.G., Heusinkveld, B.G., Holtslag, A.A.M., 2007. Seasonal and interannual variability of carbon dioxide and water balance over a grassland. *Clim. Change* 82, 163–177.
- Jacobs, C.M.J., de Bruin, H.A.R., 1997. Predicting regional transpiration of elevated atmospheric CO_2 : influence of the PBL-vegetation interaction. *J. Appl. Meteorol.* 36, 1663–1675.
- Janssen, R.H.H., Vilà-Guerau de Arellano, J., Jimenez, J.L., Ganzeveld, L.N., Robinson, N.H., Allan, J.D., Coe, H., Pugh, A.M., 2012. Influence of boundary layer dynamics and isoprene chemistry on the organic aerosol budget in a tropical forest. *J. Geophys. Res.* 118, 9351–9366.
- Katul, G.G., Ellsworth, D.D., Lai, C., 2000. Modelling assimilation and intercellular CO_2 from measured conductance: a synthesis of approaches. *Plant Cell Environ.* 23, 1313–1328.
- Lambers, H., Chapin III, F.S., Pons, T.L., 2008. *Plant Physiological Ecology*. Springer.
- Lee, X., Griffis, T.J., Baker, J.M., Billmark, K.A., Kim, K., Welp, L.R., 2009. Canopy-scale kinetic fractionation of atmospheric carbon dioxide and water vapor isotopes. *Glob. Change Biol.* 103, GB1002.
- Lee, X., Huang, J., Patton, E.G., 2012. A large-eddy simulation study of water vapor and carbon dioxide isotopes in the atmospheric boundary layer. *Bound. Layer Meteorol.* 145, 229–248.
- Leuning, R., van Gorsel, E., Massman, W.J., Isaac, P.R., 2018. Reflection on the surface energy imbalance. *Agric. For. Meteorol.* 156, 65–74.
- Lilly, D.K., 1968. Models of cloud-topped mixed layers under strong inversion. *Q. J. R. Meteorol. Soc.* 94, 292–309.
- Moene, A.F., van Dam, J.C., 2014. *Transport in the Atmosphere-Vegetation-Soil Continuum*. Cambridge University Press.
- Monson, R., Baldocchi, D., 2014. *Terrestrial Biosphere-Atmosphere Fluxes*. Cambridge University Press.
- Moore, K.E., Fitzjarrald, D.R., Sakai, R.K., Goulden, M.L., Munger, J.W., Wofsy, S.C., 1996. Seasonal variation in radiative and turbulent exchanges at a deciduous forest in central Massachusetts. *J. Appl. Meteorol.* 35, 122–134.
- Ouwersloot, H.G., Vilà-Guerau de Arellano, J., Nölscher, A.C., Krol, M., Ganzeveld, L.N., Breitenberger, C., Mammarella, I., Wiliams, J., Lelieveld, J., 2012. Characterization of a boreal convective boundary layer and its impact on atmospheric chemistry during HUMPPAC-COPEC-2010. *Atmos. Chem. Phys.* 12, 9335–9353.
- Pedruzo-Bagazgoitia, X., Ouwersloot, H.G., Sikma, M., van Heerwaarden, C.C., Jacobs, C.M.J., Vilà-Guerau de Arellano, J., 2017. Direct and diffuse radiation in the shallow cumulus-vegetation system: enhanced and decreased evapotranspiration regimes. *J. Hydrometeorol.* 18, 1731–1748.
- Reichstein, M., Falge, E., Baldocchi, D., Papale, D., Aubinet, M., Berbigier, P., Bernhofer, C., Buchmann, N., Gilmanov, T., Granier, A., Grinwald, T., Havrankova, K., Ilvesniemi, H., Janous, D., Knol, A., Laurila, T., Lohila, A., Loustau, D., Matteucci, G., Meyers, T., Miglietta, F., Ourcival, J.M., Pumpanen, J., Rambal, S., Rotenberg, E., Sanz, M., Tenhunen, J., Seufert, G., Vaccari, F., Vesala, T., Yakir, D., Valentini, R., 2005. On the separation of net ecosystem exchange into assimilation and ecosystem respiration: review and improved algorithm. *Glob. Change Biol.* 11, 1424–1439. <https://doi.org/10.1111/j.1365-2486.2005.001002.x>
- Risk, D., Kellman, L., Beltrami, H., 2002. Carbon dioxide in soil profiles: production and temperature dependence. *Geophys. Res. Lett.* 29. <https://doi.org/10.1029/2001GL014002>.
- Ronda, R.J., de Bruin, H.A.R., Holtslag, A.A.M., 2001. Representation of the canopy conductance in modeling the surface energy budget for low vegetation. *J. Appl. Meteorol.* 40, 1431–1444.
- Sturm, P., Eugster, W., Knol, A., 2012. Eddy covariance measurements of CO_2 isotopologues with a quantum cascade laser absorption spectrometer. *Agric. For. Meteorol.* 152, 73–82.
- Tennekes, H., Driedonks, A.G.M., 1981. Basic entrainment equations for the atmospheric boundary layer. *Bound. Layer Meteorol.* 20, 515–531.
- Trenberth, K.E., Fasullo, J.T., Kiehl, J., 2000. Earth's global energy budget. *Bull. Am. Meteorol. Soc.* 90, 311–323.
- van Heerwaarden, C.C., Vilà-Guerau de Arellano, J., Gounou, A., Guicard, F., Couvreux, F., 2010. Understanding the daily cycle of evapotranspiration: a method to quantify the influence of forcing and feedback. *J. Hydrometeorol.* 11, 1405–1422.
- Van Kesteren, B., Hartogensis, O.K., van Dinther, D., Moene, A.F., de Bruin, H.A.R., 2013. Measuring H_2O and CO_2 fluxes at field scales with scintillometry. Part II: Validation and application of 1-min flux estimates. *Agric. For. Meteorol.* 178, 88–105.
- Vilà-Guerau de Arellano, J., Gioli, B., Miglietta, F., Jonker, H., Baltink, H., Hutzler, R., Holtslag, A., 2004. Entrainment process of carbon dioxide in the atmospheric boundary layer. *J. Geophys. Res.* 109, D18110.
- Vilà-Guerau de Arellano, J., van Heerwaarden, C.C., van Stratum, B.J.H., van den Dries, K., 2015. *Atmospheric Boundary Layer: Integrating Air Chemistry and Land Interactions*. Cambridge University Press.
- Vilà-Guerau de Arellano, J., van Heerwaarden, C.H., Lelieveld, J., 2012. Modelled suppression of boundary-layer clouds by plants in a CO_2 -rich atmosphere. *Nat. Geosci.* 5, 701–704.
- Vinuesa, J.F., Vilà-Guerau de Arellano, J., 2003. Fluxes and (co-)variances of reacting scalars in the convective boundary layer. *Tellus B* 55, 935–949.
- Wehr, R., Munger, J.W., Nelson, D.D., McManus, J.B., Zahniser, M.S., Wofsy, S.C., Saleska, S.R., 2013. Long-term eddy covariance measurements of the isotopic composition of the ecosystem-atmosphere exchange of CO_2 in a temperate forest. *Agric. For. Meteorol.* 181, 69–84.
- Wehr, R., Saleska, S.R., 2015. An improved isotopic method for partitioning net ecosystem-atmosphere CO_2 exchange. *Agric. For. Meteorol.* 214–215, 515–531.
- Werner, C., Schnyder, H., et al., 2012. Progress and challenges in using stable isotopes to trace plant carbon and water relations across scales. *bgs* 9, 3083–3111.
- Wofsy, S.C., Goulden, M., Manager, J., Fan, S., Bakwin, P., Daube, B., Bassow, S., Bazza, F., 1993. Net exchange of CO_2 in a mid-latitude forest. *Science* 260, 1314–1317.
- Wu, H., Lee, X., 2011. Short-term effects of rain on soil respiration in two New England forests. *Plant Soil* 338, 329–342.
- Yakir, D., Sternberg, L.S.L., 2000. The use of stable isotopes to study ecosystem gas exchange. *Oecologia* 123, 297–311.
- Zhang, X.P., Yang, Z.L., Niu, G.Y., Wang, X.Y., 2009. Stable water isotope simulation in different reservoirs of Manaus, Brazil by Community Land Model incorporating stable isotope effect. *Int. J. Climatol.* 29, 619–628.